ARMY RESEARCH LABORATORY

Helicopter-Mounted Laser Beam Characterization Test 2

by Fernando R. Palacios
Wendell R. Watkins
Samuel B. Crow
Daniel R. Billingsley
Battlefield Environment Directorate

ARL-TR-825

January 1996

NOTICES

Disclaimers

The findings in this report are not to be construed as an official Department of the Army position, unless so designated by other authorized documents.

The citation of trade names and names of manufacturers in this report is not to be construed as official Government indorsement or approval of commercial products or services referenced herein.

Destruction Notice

When this document is no longer needed, destroy it by any method that will prevent disclosure of its contents or reconstruction of the document.

DISCLAIMER NOTICE

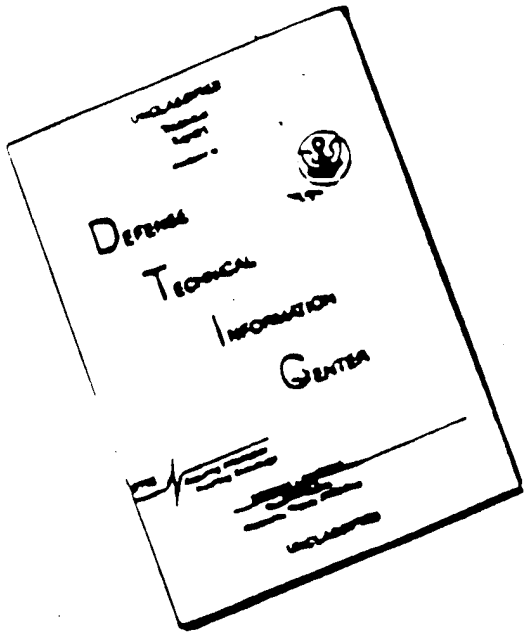

THIS DOCUMENT IS BEST QUALITY AVAILABLE. THE COPY FURNISHED TO DTIC CONTAINED A SIGNIFICANT NUMBER OF PAGES WHICH DO NOT REPRODUCE LEGIBLY.

REPORT DOCUMENTATION PAGE

Form Approved
OMB No. 0704-0188

1. AGENCY USE ONLY (Leave blank)	2. REPORT DATE	3. REPORT TYPE AND DATES COVERED
	January 1996	Final

4. TITLE AND SUBTITLE

Helicopter-Mounted Laser Beam Characterization Test 2

5. FUNDING NUMBERS

6. AUTHOR(S)

Fernando R. Palacios, Wendell R. Watkins, Samuel B. Crow,
Daniel E. Billingsley

7. PERFORMING ORGANIZATION NAME(S) AND ADDRESS(ES)

U.S. Army Research Laboratory
Battlefield Environment Directorate
Attn: AMSRL-BE-S
White Sands Missile Range, NM 88002-5501

8. PERFORMING ORGANIZATION REPORT NUMBER

ARL-TR-825

9. SPONSORING/MONITORING AGENCY NAME(S) AND ADDRESS(ES)

U.S. Army Research Laboratory
2800 Powder Mill Road
Adelphi, MD 20783-1145

10. SPONSORING/MONITORING AGENCY REPORT NUMBER

ARL-TR-825

11. SUPPLEMENTARY NOTES

12a. DISTRIBUTION/AVAILABILITY STATEMENT

Approved for public release; distribution is unlimited.

12b. DISTRIBUTION CODE

A

13. ABSTRACT *(Maximum 200 words)*

The effectiveness of a laser designator is dependent on the intensity and size of the beam placed on a target. This report describes a laser beam spread ansd wander test conducted at Holloman Air Force Base on August 18, 1994, by the Army Research Laboratory. To assess the performance of a helicopter-mounted laser, the beam was characterized by viewing and analyzing the diffuse reflections from a target board. The results are compared to a similar test conducted on June 7, 1994. Measurements were made to determine the impact of the platform (on which the laser designator was mounted) and environment on beam characteristics for a helicopter-mounted mid-infrared (IR) laser. A large reflective surface (2.44 by 2.44 m) target board was used to determine beam size and intensity. The board contained a hot blackbody (IR) source to guide the laser tracking system in directing the laser beam to its surface. The 30-Hz-frame-rate, mid-IR imager was used to characterize the diffuse reflections of the 100-kHz, repetively pulsed, mid-IR laser beam. Data were recorded for the helicopter engine on/off, different hovering altitudes, and different ranges from the helicopter to the stationary reflective target board. When the helicopter was on the ground at 500-m range and with strong optical turbulence, there was some decrease in the beam spreading when the helicopter rotor was on, compared to when the rotor was off. When the helicopter was hovering and rotated so the exhaust and laser were pointed toward the target board, there was a bimodal beam geometry formed that changed shape with range and, presumably, is related to the air compression changes caused by the rotor downwash and refractive index changes in the exhaust plume.

14. SUBJECT TERMS

laser beam characterization

15. NUMBER OF PAGES

64

16. PRICE CODE

17. SECURITY CLASSIFICATION OF REPORT	18. SECURITY CLASSIFICATION OF THIS PAGE	19. SECURITY CLASSIFICATION OF ABSTRACT	20. LIMITATION OF ABSTRACT
Unclassified	Unclassified	Unclassified	SAR

Acknowledgments

The authors thank Aviation System Command and Holloman Air Force Base for their assistance in setting up and running the test.

Contents

Figures

Tables

1. Introduction

A laser beamspread and wander test was conducted at Holloman Air Force Base (HAFB) on June 7, 1994 by the Army Research Laboratory (Palacios et al. 1994). Measurements determined the impact of the helicopter-mounted laser platform and environment on propagation characteristics for a mid-infrared (IR) laser. A large reflective surface (2.44- by 2.44-m) target board was used to determine beam size and intensity. The board contained a beam directing mirror reflecting a hot blackbody (IR) source to guide the laser tracking system toward the target board (figure 1). The 30-Hz frame rate, model 610 Inframetrics imager from the Battlefield Environment Directorate Mobile Imaging Spectroscopy Laboratory was used to characterize the diffuse reflections of the 100-KHz, repetitively-pulsed, mid-IR laser beam from the target board surface. Data were recorded for the helicopter engine on/off, different helicopter altitudes, and different ranges from the helicopter to the stationary reflective target board. Several references describe characteristics of the imager and image processing techniques (Inframetrics 1983; Jordan 1994; Kantrowitz et al. 1990; Crow et al. 1991; Watkins et al. 1989; Palacios et al. 1992).

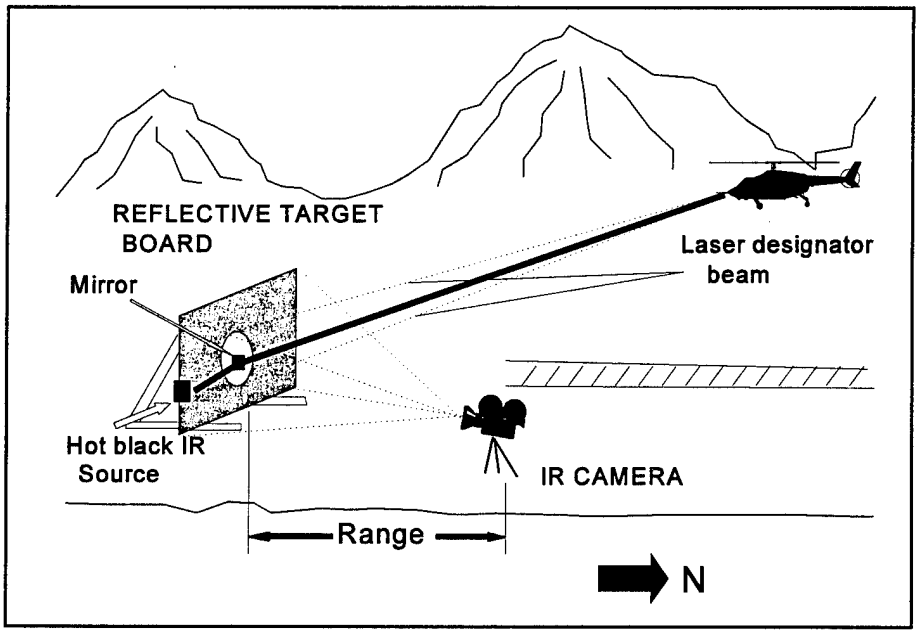

Figure 1. Experimental setup for June (R = 28 m) and August (R = 47 m) tests.

Although much useful information was derived from the June test, a second test was needed. The second test was conducted on August 18, 1994 at HAFB. Figure 1 shows the basic experimental setup for the June and August tests, and tables 1 and 2 give the test results. For the June test, the imager was positioned to the east of the rocket sled at a range of 28 m, and no magnifying telescope lens was used. For the August test, the imager was positioned to the west of the sled at a range of 47 m, and a 6.7X telescope lens was used. To align the laser beam on the target board, a hot blackbody and 10-cm effective diameter right angle parabolic mirror were used. For the August test, the mirror was mounted on the left side of the target (as viewed from the front) to direct the blackbody radiation toward the laser tracker of the helicopter, because the laser beam was intentionally offset by about ½ m to the right at a 250-m range. The mirror was used to prevent the blackbody radiation from biasing the measurements of the beam-spread and wander imagery. As it turned out, the mirror position was not optimum because the laser tracker aim point was shifted left nearly 1 m at a range of 500 m (about a 2 mrad offset), and the beam became nonGaussian in intensity distribution for the exhaust plume tests. Of the imagery collected, 14 trials were used to analyze the laser beam on the target board.

One shortcoming of the June test was the decreased signal-to-noise level produced by solar loading on the target board. A large tent was constructed to house the entire target board to eliminate this problem. Also, the resolution and sensitivity of the imagery were improved for the August test by using a 6.7X telescope to isolate the target board in the IR scene. No turbulence data were collected at the June test, so a scintillometer was set up at 2-m elevation to measure the C_n^2 value over a 1-km path along the sled track. A computer was scheduled to collect the scintillometer data, but the 40+ °C temperatures caused the computer and encoder to malfunction. The scintillometer was showing a value of C_n^2 in the mid 10^{-13} $m^{-2/3}$. The lack of time encoding for the imagery (also caused by hot weather equipment failure) caused problems in analyzing the data. One problem that caused more severe consequences was the skewing of the laser beam caused by the misalignment of the laser beam tracker on the target board by the helicopter mounted laser pointer. (The laser pointer in the August test was different from the June test.) The skewing problem is addressed later. In spite of the difficulties encountered, the August

test produced some useful results; effects of the platform and environmental condition on the laser beam characteristics were determined.

Discussion of the test results begin with the hovering trials in which minimal beam spread and wandering is expected. The medium range ground trials are described to show the effects of the ground-level optical turbulence. Medium and far range trials with and without exhaust turbulence are analyzed to show the effects of the range and the exhaust turbulence.

Table 1. June test beam-spread and wander parameters

Trial	Min[a] (GS)	Max[b] (GS)	Mag[c] (GS)	Effective Diameter pixels	Nominal (Wd) pixels	Nominal (Ht) pixels	Nominal Diameter pixels	Stretch (Ht/Wd)	Relative Energy
1[d]	32	260	228	45.4	51	45	47.9	0.88	1.00
2[e]	35	240	205	46.7	43	48	45.4	1.12	0.95
3[e]	34	250	216	47.0	41	55	47.5	1.34	1.02
4[f]	39	300	261	51.4	45	57.5	50.9	1.28	1.47
5[f]	36	250	214	52.4	41	56.5	48.1	1.38	1.25
6[g]	40	120	80	57.1	45	100	67.1	2.22	0.56
7[g]	40	140	100	53.6	39	78.5	55.3	2.01	0.61
8[h]	28	250	222	47.4	35.5	50	42.1	1.41	1.06
9[i]	32	300	268	55.6	35	78	52.2	2.23	1.76

[a]Grayscale value for the background.

[b]Grayscale value for the peak beam temperature.

[c]Grayscale value for the peak beam temperature above the background.

[d]Trial 1 was at 343-m range with the helicopter on the ground and rotors off.

[e]Trials 2 and 3 were at 343-m range with the helicopter on the ground with the rotors on.

[f]Trials 4 and 5 were at 343-m range with the helicopter hovering at an elevation of 20 m.

[g]Trials 6 and 7 were at 680-m range with the helicopter hovering at an elevation of 20 m.

[h]Trial 8 was the same as trials 4 and 5 except that the helicopter line of sight to the target board was on the same side of the target board surface normal.

[i]Trial 9 was from the same line of sight as trial 8 through the helicopter exhaust.

Table 2. August test beam-spread and wander parameters

Trial	Min[a] (GS)	Max[b] (GS)	Mag[c] (GS)	Effective Diameter pixels	Nominal (Wd) pixels	Nominal (Ht) pixels	Nominal Diameter pixels	Stretch (Ht/Wd)	Relative Energy
1[d]	13	222	222	122.4	107	140	122.4	1.31	1.06
2[d]	16	235	219	116.0	99	125	111.2	1.26	0.94
3[e]	15	232	217	133.2	115.5	126	120.6	1.09	1.23
4[e]	15	237	222	135.1	129.5	123.5	126.5	0.95	1.29
5[f]	22	177	155	92.8	72.5	112	90.1	1.54	0.42
6[f]	22	192	170	87.9	69	111	87.5	1.61	0.42
7[g]	22	146	124	73.8	57	95	73.6	1.67	0.22
8[h]	23	190	167	88.1	76.5	111	92.1	1.45	0.41
9[h]	21	184	163	88.8	91	140	112.9	1.54	0.41
10[i]	19	183	164	86.8	91	109.5	99.8	1.20	0.39
11[j]	22	113	91	79	69	158	104.4	2.29	0.18
12[j]	20	110	90	81.7	79.5	150	109.2	1.89	0.19
13[k]	N/A	N/A	N/A	N/A	N/A	N/A	N/A	N/A	N/A
14[k]	N/A	N/A	N/A	N/A	N/A	N/A	N/A	N/A	N/A

[a]Grayscale value for the background.

[b]Grayscale value for the peak beam temperature.

[c]Grayscale value for the peak beam temperature above the background.

[d]Trials 1 and 2 were at 250-m range with the helicopter hovering at 20-m elevation.

[e]Trials 3 and 4 were at 250-m range with the helicopter hovering at 20-m elevation with the beam passing through the exhaust.

[f]Trials 5 and 6 were at 500-m range with the helicopter on the ground with the rotors on.

[g]Trial 7 was at 500-m range with the helicopter on the ground with the rotors off.

[h]Trials 8 and 9 were at 500-m range with the helicopter hovering at a 20-m elevation.

[i]Trial 10 was at 500-m range with the helicopter hovering at 20-m elevation with the beam passing through the exhaust.

[j]Trials 11 and 12 were at 750-m range with the helicopter hovering at a 20-m elevation.

[k]Trials 13 and 14 were at 750-m range with the helicopter hovering at a 20-m elevation with the beam passing through the exhaust.

2. Experimental Approach

The analyses approach used during the June test is presented first. To obtain the best signal-to-noise ratio, the imager was set on the most sensitive grayscale (GS) range (5 °C separated into 256-levels). The coolest portion of the target board was set to the lowest GS level. The laser-produced hot spots, typically, were not saturated, although some saturation occurred and had to be dealt with during data reduction, as discussed later. Figure 2 shows an example of an image from the June test. The time is encoded in the rectangle at the top center of the image. The image is a 256 by 256 representation of the 4:3 aspect of the analog signal scene. The whole image has 320 by 240 pixels; therefore, the digitized image contains only about 80 percent of the width and has an extra margin at the bottom containing no scene information. In addition, there are only 200 lines of actual detector scanned information are in each image. The imager was operated to scan only 40 percent of its full field of view extent; therefore, the image is only 8° in width instead of 20°. Of the 65 K pixels in the image, about 40 K (200 by 200) comprise the target board area with a background on the left side. The target board had some direct solar illumination on the upper left corner because it was not shielded from the sun; therefore, the laser beam was positioned on the lower right during the June test (figure 2). The first trial of the June test was for the helicopter on the ground at a range of 343 m with the rotor engine off. The line of sight to the helicopter was about 2° west of the north-south rocket sled track with the target board on the south end; whereas, the line of sight to the imager was about 5° east of the track.

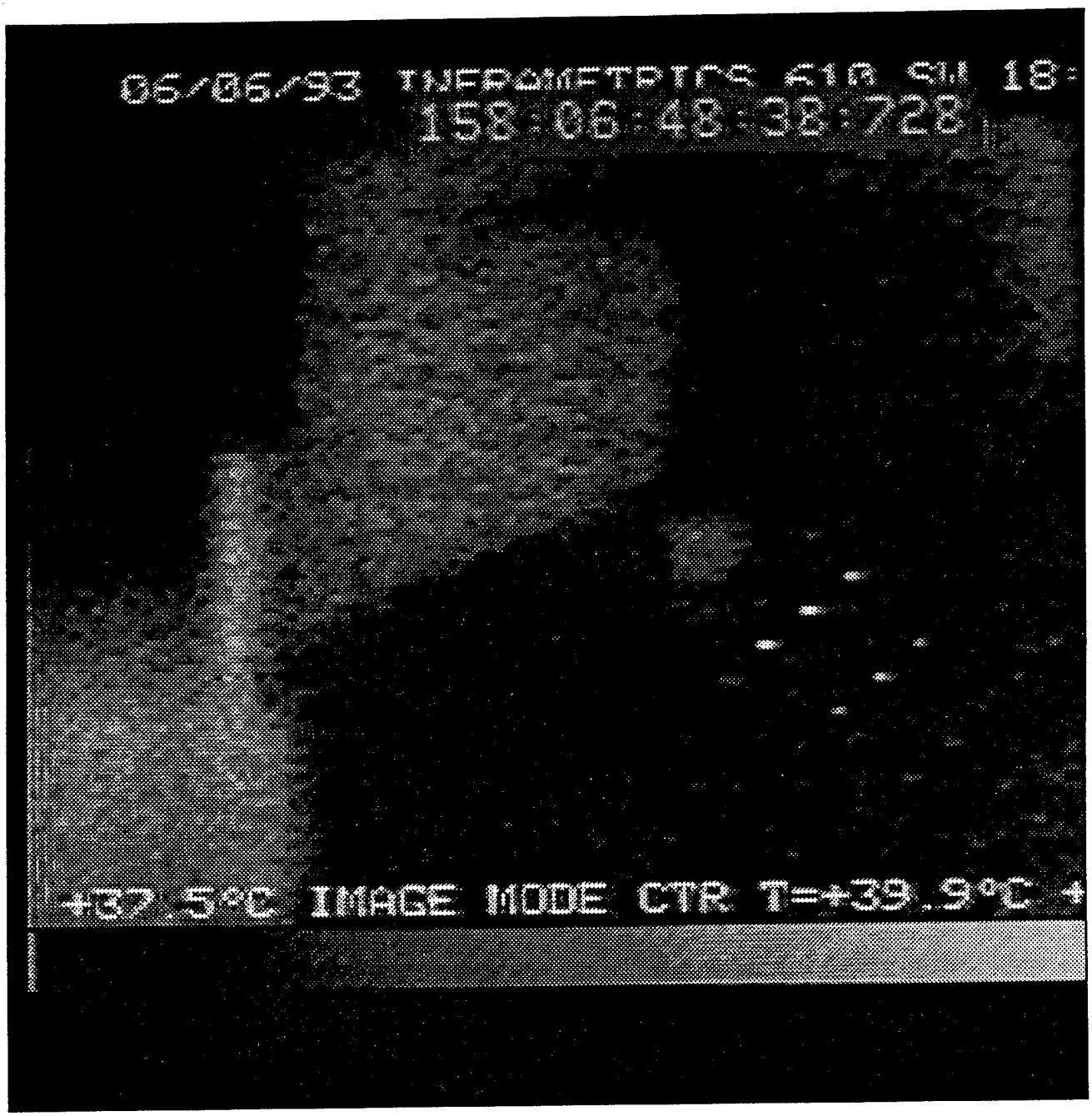

Figure 2. Single-element scanning detector image containing laser hot spots from June trial 1.

Determining the actual laser beam spreads from a set of images, like the one in figure 2, was not a trivial task. First, sets of 50 consecutive images were digitized. A simple averaging of images to reduce noise and enhance the signal did not work because most of the laser hot spots did not overlap from frame to frame. (The hot spots ended up blending into the background GS levels.) Therefore, a maximizing utility was used to examine the pixel gray levels of the image, select a maximum value for each row and column of the images gathered, and place the value in a destination image. Before this operation was performed, the scene feature was minimized by taking the absolute difference between a 50-frame average of the target scene just before the laser was turned on, as shown in figure 3, and the individual laser beam images illustrated by figure 2. Figure 4 is the result of the maximizing utility for the 50 laser beam images. Not all the feature details disappeared, and the warmer regions, such as the upper left portion of the target board, had more variation than the cooler portions. The laser beam spread is clearly visible in figure 4 with a slightly truncated Gaussian beam shape with a tail trailing off to the right. One point should be made with respect to the average beam images: two spots at the center of the left-hand side of the image were caused by the mirror holder, preventing complete cancellation between the average background image and the laser beam images.

To fill the gaps in the beam, a maximizing filter was used to replace the image pixel values in every 3- by 3-pixel grid by the maximum GS value in the individual 9-pixel grid. The process was performed three times, shifting the grid lattice over and down one pixel each time. Figure 5 shows the results. To remove the blockish image edges in figure 5, a smoothing filter was applied three times. Figure 6 shows the results. Figure 6 shows a very good representation of the laser beam pattern. The representation was used in subsequent analyses. Because of an intensity increase when the laser is first turned on, the laser beam images were collected beginning approximately 1 s after the beam appeared on the target board.

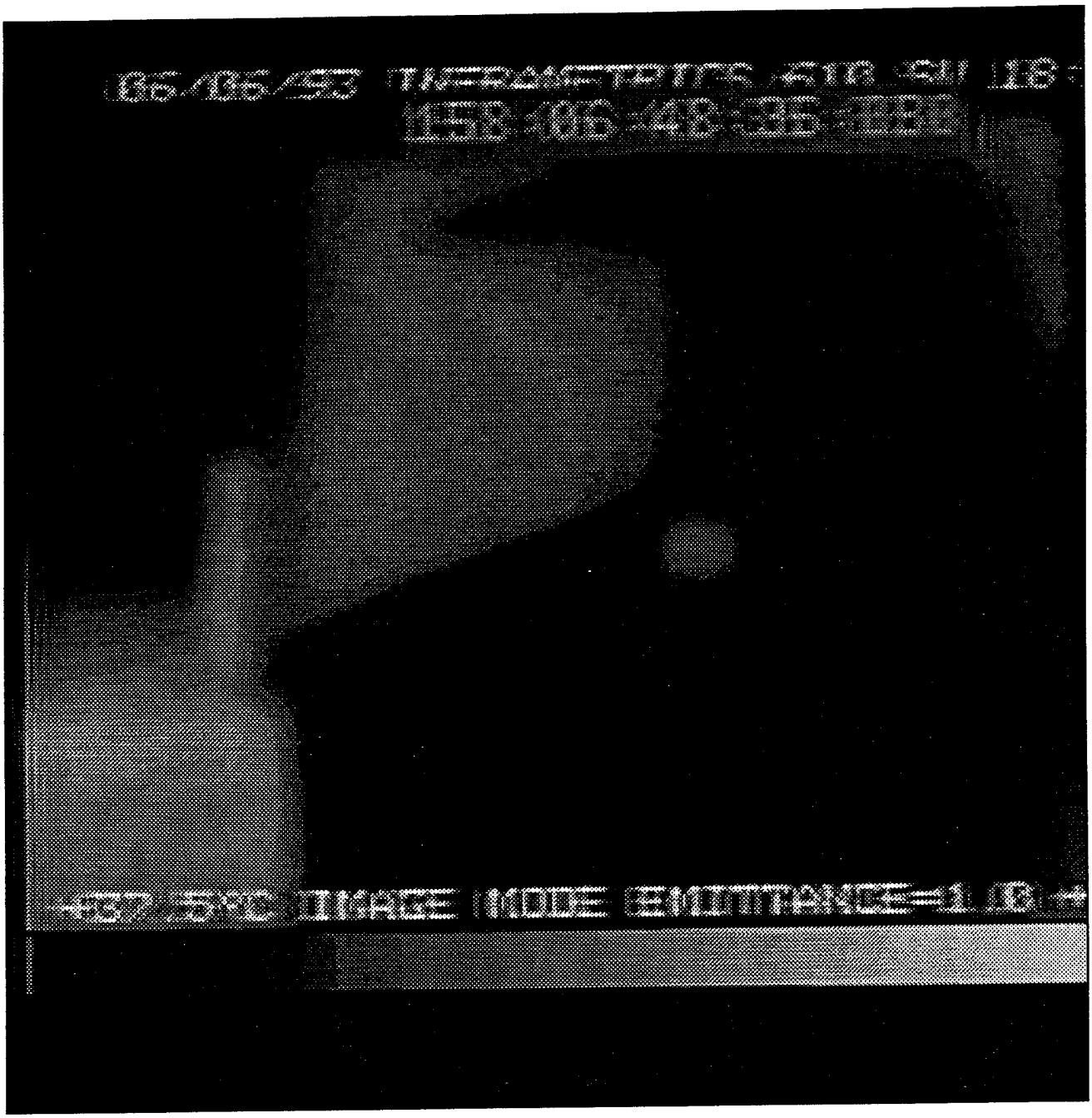

Figure 3. Image of 50-frame average of target scene before the laser was turned on in June trial 1.

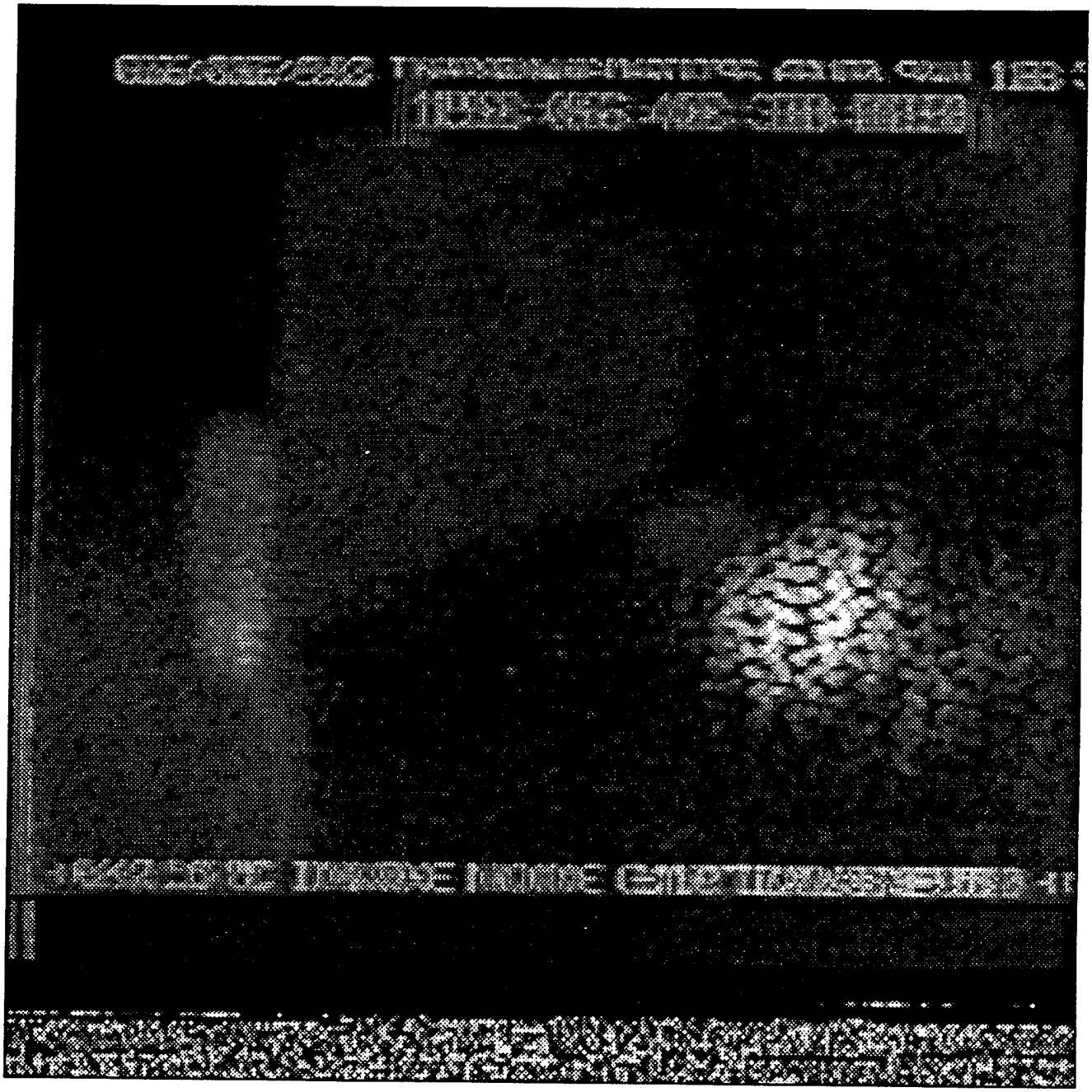

Figure 4. Maximizing utility image for 50 laser beam images captured in June trial 1.

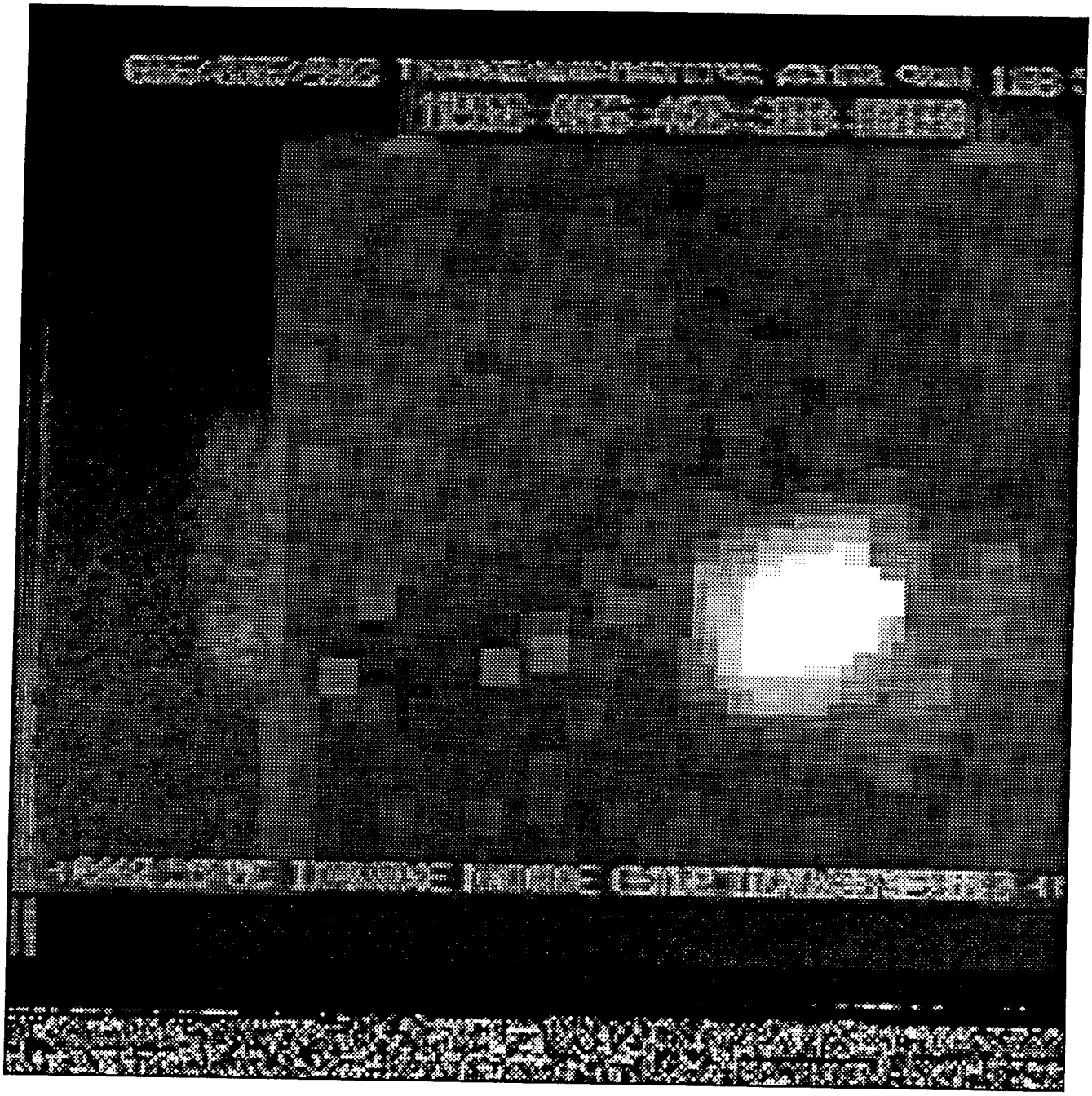

Figure 5. Maximizing filter image derived from the maxmizing utility image in June trial 1.

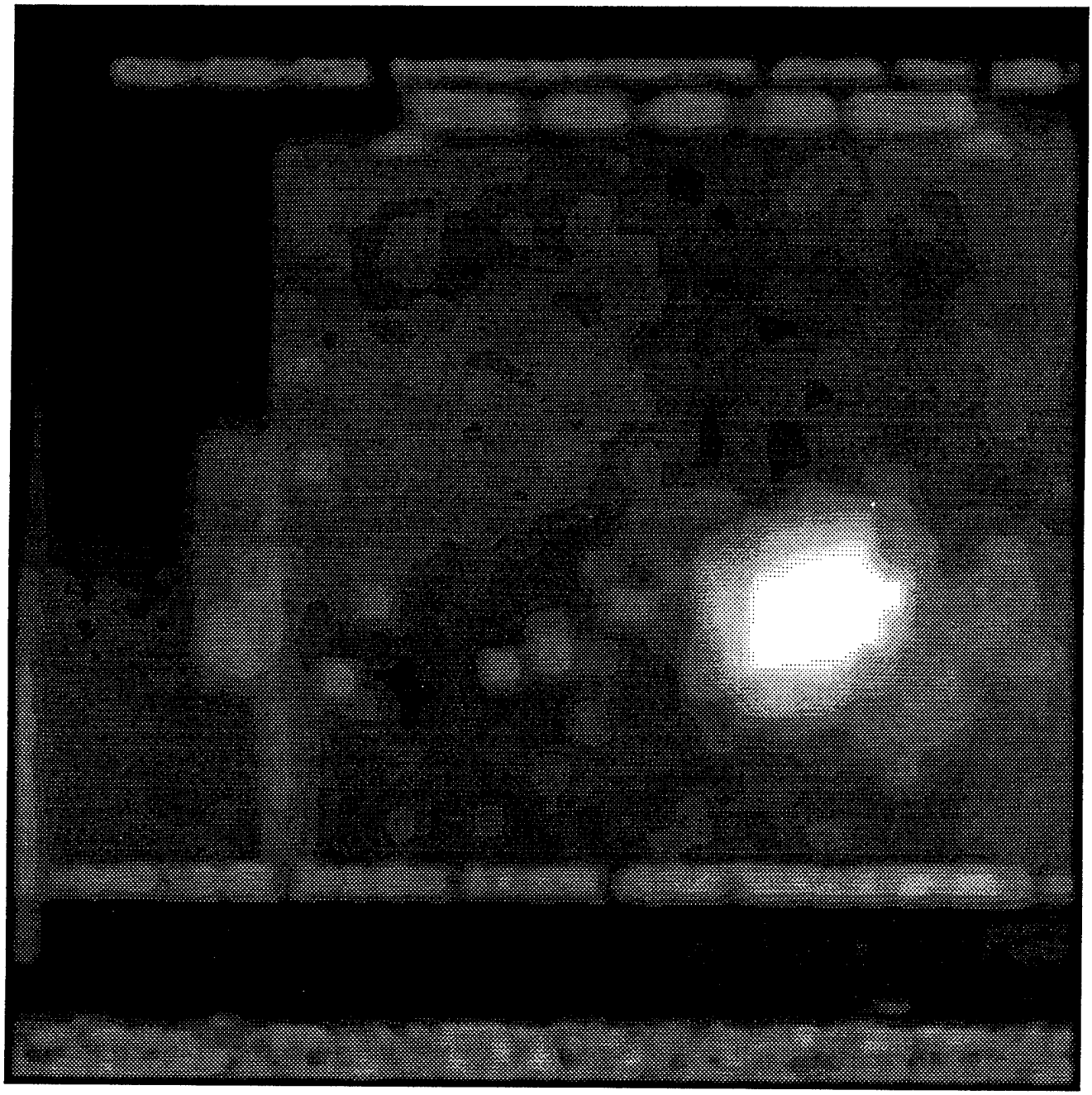

Figure 6. Smoothing function image derived from the maximizing filter image in June trial 1.

Some profiles were truncated because of saturation. A scheme was developed to estimate the true peak or maximum to overcome the saturation problem. First, the background level (minimum) was derived by isolating the laser beam (using a 2X image processing zoom of the laser beam area) and determining the 10 percent threshold GS level. During the first June trial, the minimum GS was 32 (table 1). By comparing the truncated and nontruncated trials, the truncated beam maximum could be derived by extrapolation. For trial 1, the resulting maximum value was 260 and yielded a beam magnitude of 228 GS values (260 - 32).

The smoothing function and maximizing filter used on images altered the original shape and GS intensity of the laser beam. For example, a circle of GS 205 and a background of zero is represented in figure 7a. Figure 7b through d shows the influence on the circle caused by the smoothing function, maximizing filter, and a combination of both. The smoothing function (figure 7b) caused the circle to increase in size by 34.30 percent, but decreased the intensity of maximum magnitude (205 GS) pixels by 67 percent, as detailed in table 3. Although the circle increased in size, it actually appears smaller, because the background was averaged with the circle in the smoothing function. The maximizing filter increased the area nonuniformly 49.48 percent and the intensity 49.48 percent. A combination of the maximizing filter and smoothing function increased the area and intensity by 91.62 and 11.11 percent, respectively.

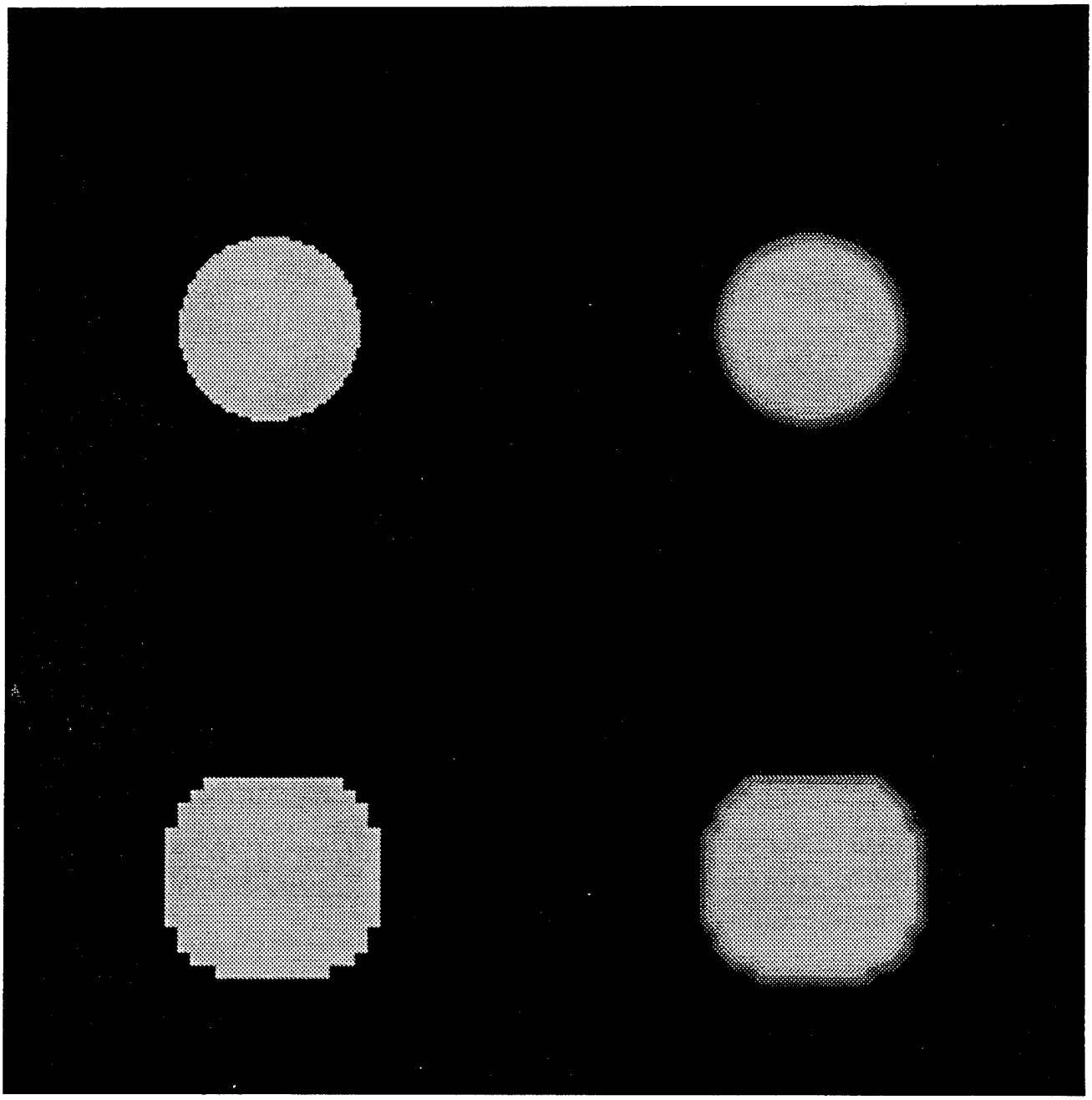

Figure 7. a) Circle of GS 205 and background zero (top left); b) Circle a smoothed three times (top right); c) Circle a maximized filtered three times (bottom left); d) Circle a maximized filtered and smoothed three times (bottom right).

Table 3. Circle analyses

Area Analyses	Circle	Circle Smooth X 3	Maximizing Filter X 3	Maximizing Filter X 3 Smooth X 3
Histogram % Pixels GS Zero (Min)	97.777 % 64,079 pixels	7.014 % 63,579 pixels	96.677 % 63,358 pixels	95.740 % 62,744 pixels
Histogram % Pixels GS 205 (Max)	2.223 % 1,457 pixels	1.491 % 977 pixels	3.323 % 2178 pixels	2.472 % 1620 pixels
100%-(Max+Min)	0 %	1.495 % 980 pixels	0 %	1.788 % 1,172 pixels
% Circle Area Increase	0 %	34.30 %	49.48 %	91.62 %
% Circle Area 205 GS Increase	0 %	-67.0 %	49.48 %	11.11 %

The maximizing and smoothing routine matches the maximum GS (intensity) to the circle area and most closely represents the circle. The smoothing function alone does represent the laser beam because of the gaps between hot spots in the maximized utility images (figure 4) and the loss in the intensity of maximum magnitude pixels of the beam. Figure 8a through d shows the actual laser beams in trial 1 manipulated similarly to the circles in figure 7a through d; figure 9 details the results. Figure 9 shows pixel GS analyses for row 140 (at the center of each laser beam pattern in figure 8) and the respective column GS values. The maximized filtered and smoothed curve best envelopes and represents the diffuse reflected maximized utility image of the laser beam. The ideal instrument would be a staring array IR camera; however, a single-element detector (IR camera) was used due to the lack of resources. The staring array camera would give a truer representation of the diffuse reflected laser beam, although, some information about rapid changes in beam characteristics would be lost. If staring array imagery becomes available, a cross comparison of single-element detector results and the staring array results could be performed.

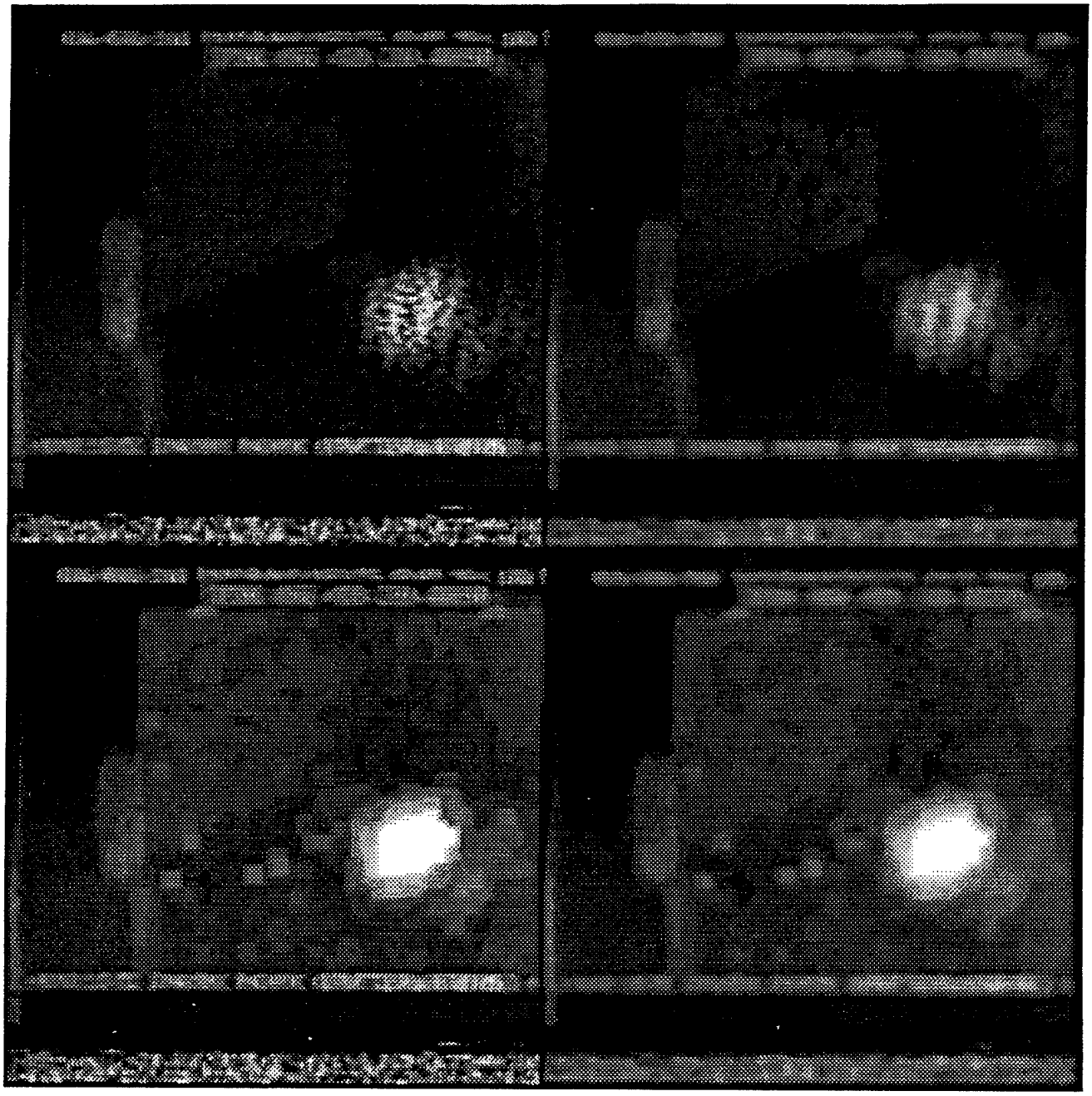

Figure 8. a) Figure 4 from June trial 1 (top left); b) Figure 4 smoothed three times (top right); c) Figure 4 maximized filtered three times (bottom left); d) Figure 4 maximized filtered and smoothed three times (bottom right).

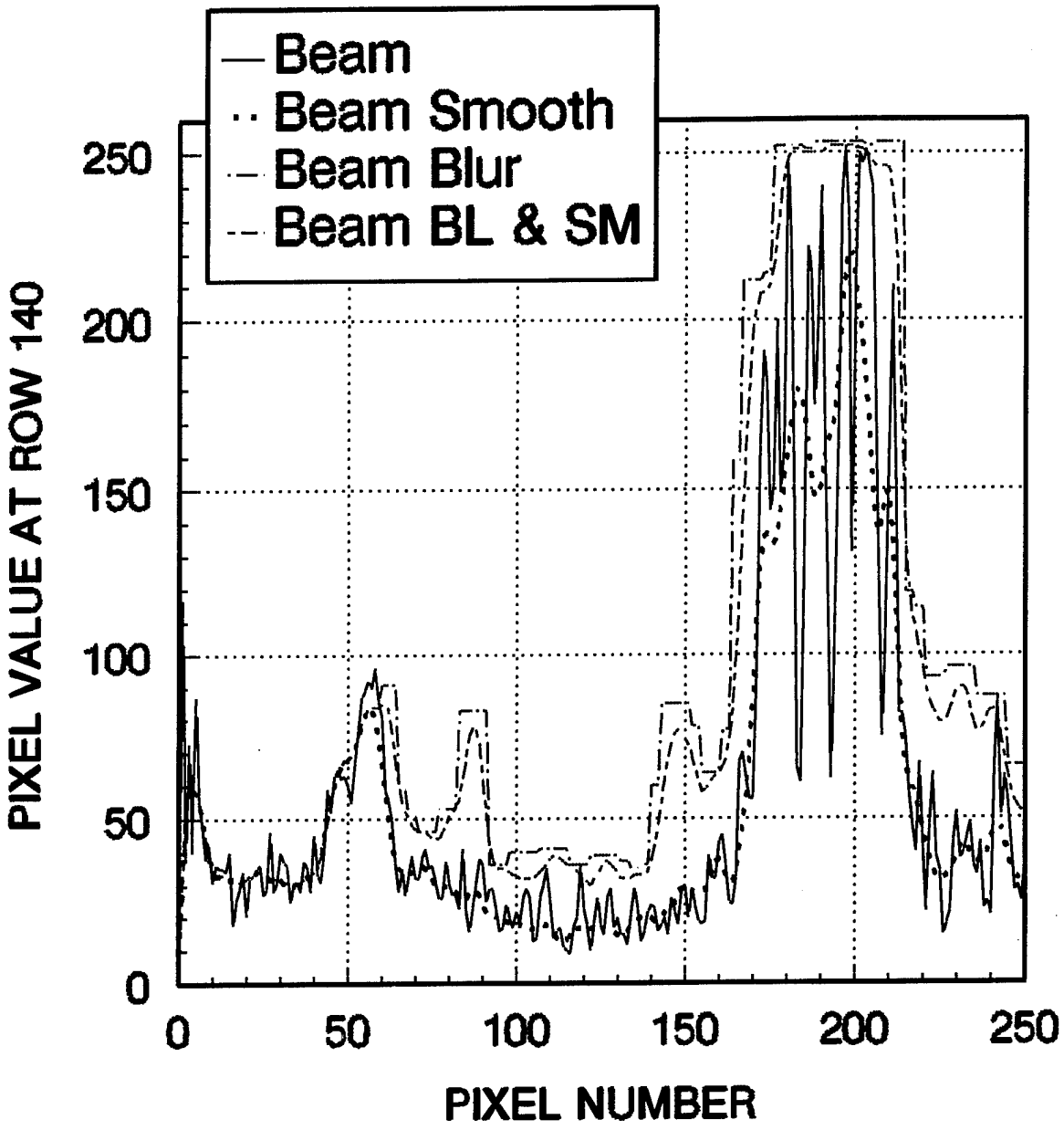

Figure 9. Pixel GS analyses for center of each beam in figure 8.

The results of the processing lead to the following conclusions. The beam is almost elliptical, but an effective full-width-at-half-maximum (FWHM) beamwidth can be assigned. An FWHM is assigned by using the half-maximum (GS level 146) threshold and deriving an effective diameter for a circle of that area (figure 10). The effective diameter, FWHM, for this trial was 45.4 pixels or about 0.4 m on the target board (because each pixel represents a square of about 0.88 cm on a side at the 28-m range). The area times the beam size was assigned a normalized beam energy (E) value of 1.0. The horizontal and vertical beam profiles were determined for the beam at FWHM and are termed the nominal width and height. For trial 1, the nominal width and height values were 51 and 45 pixels, respectively. The eccentricity (e) of the beam was derived from the beam nominal width and height (figure 10). For trial 1, the eccentricity is 0.47. Instead of limiting the eccentricity to a value of 0 to 1, the beam shapes were assigned a stretch factor of the nominal height divided by the nominal width. For trial 1, the stretch is 0.88. The area of the nominal height and width ellipse can also be used to derive a nominal diameter (here 47.9) for comparison with the effective diameter (45.4). The nominal diameters were within a few percent of the effective diameters, except for a few cases in which the beams were distorted to a nonelliptical shape. Hence, the derived stretch values are representative of the distortion of the beam.

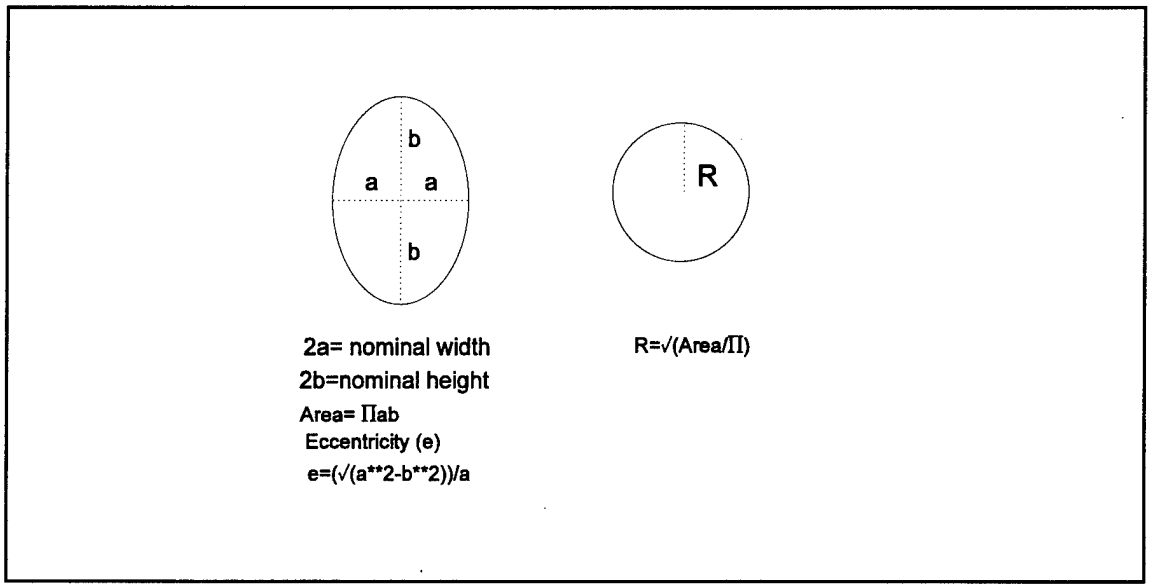

Figure 10. Ellipse and circle geometry.

3. Results of the Hovering 250-m Range (Trials 1 to 4)

This section presents a discussion of the results of the August test. The August test trials 1 through 4 are shown before trials 5 through 8 to emphasize pointing problems. The analyses technique used in the June 1994 test has been detailed (Palacios et al. 1994). At the August test, the imager was positioned on the west side of the rocket sled (figure 1) to take advantage of building shade for the electronic equipment. The positioning had no effect on the data reduction approach. Use of a 6.7X telescope to obtain more resolution and better signal-to-noise imagery had significant impact.

The imagery slightly overfills the horizontal field of view with the target board. The pixel size at the 47-m range with the full field of view and the 6.7X telescope is a square of about 0.76 cm on a side instead of the 1.22 cm for the June test in which no telescope was used. Hence, the 2.44 m on a side target board, which was about 320 pixels wide in the August test imagery, was only 200 pixels wide in the June test. In the August test, the full field of view images represent 102 K pixels in extent compared to 40 K pixels from the previous June test in which a 40 percent field of view was used. In the images, only 80 percent of the horizontal extent and 63 percent of the vertical extent of the target board are displayed (figures 11 through 14). In the images, 1 m is equivalent to about 180 pixels. With about 2½ times as many laser spots per frame, fewer frames were needed to obtain the maximized filtered laser beam pattern (30 frames for figures 11 through 14). The June test required almost twice as many frames to produce the same results. Because the original imagery data tapes were not time encoded, a significant amount of time was expended putting the time code on the audio track to allow for automating the consecutive frame grabbing and storing process.

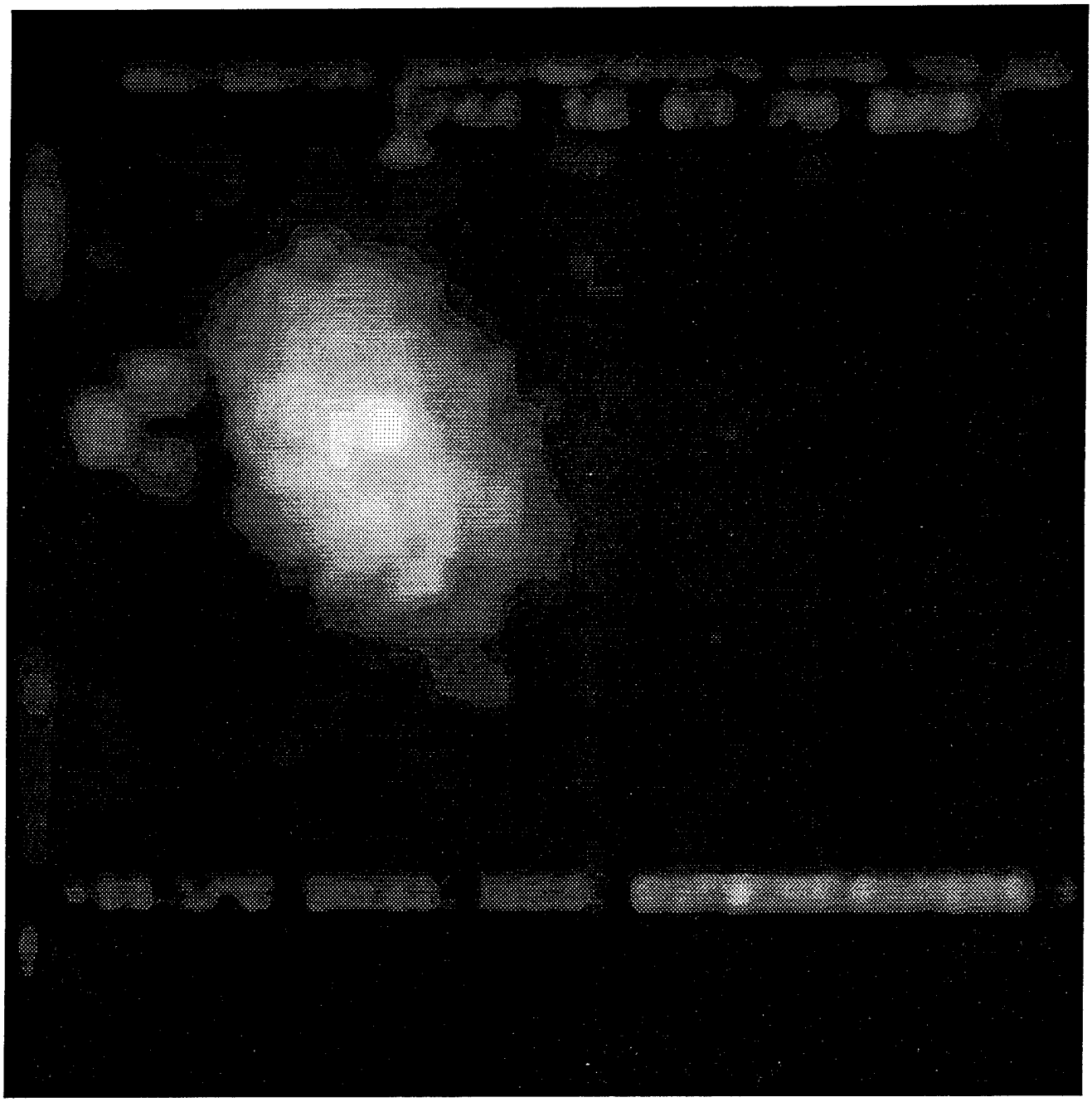

Figure 11. Thirty-frame smoothed and filtered image for trial 1 (250-m range hovering at 20-m elevation).

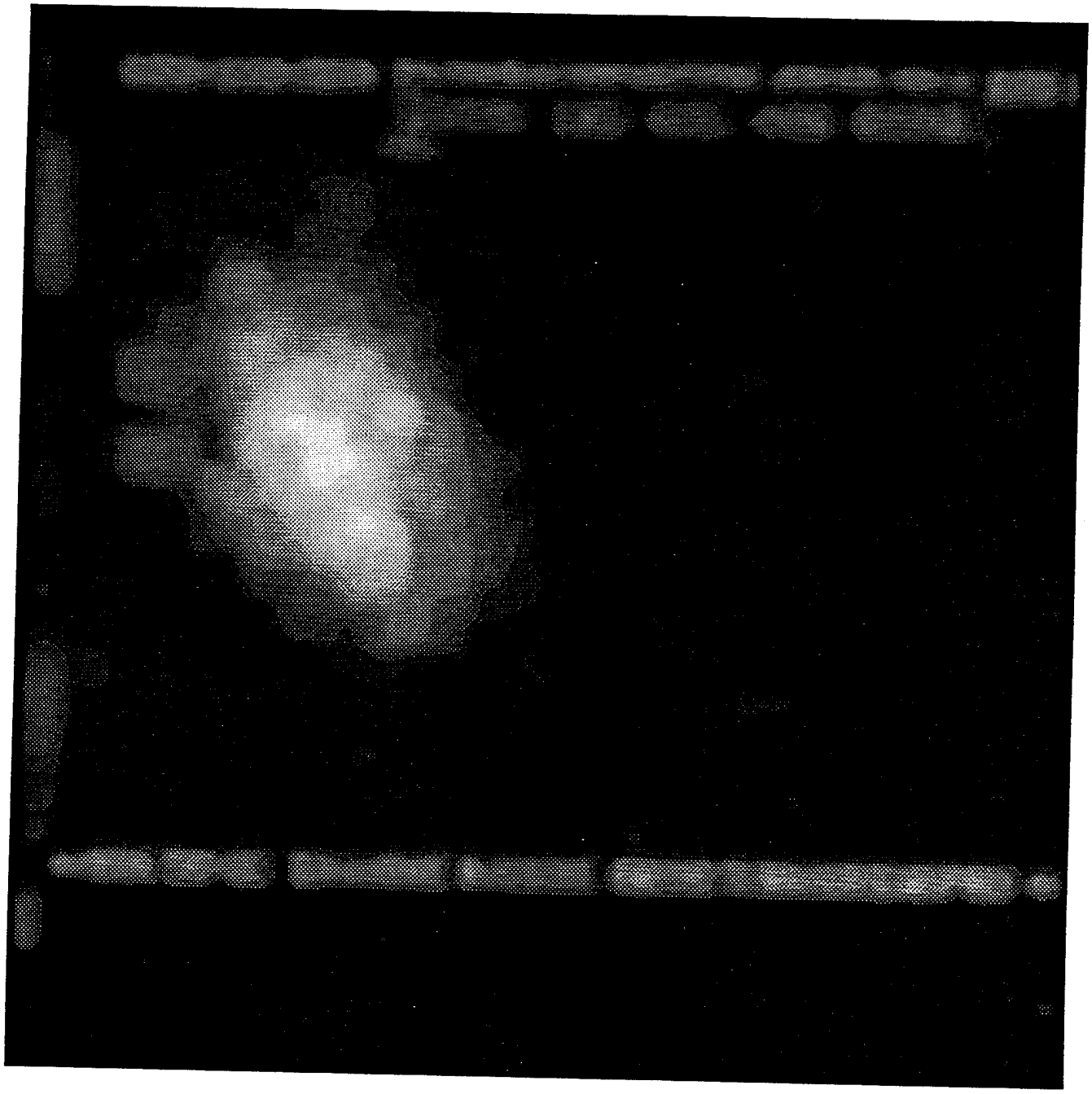

Figure 12. Thirty-frame smoothed and filtered image for trial 2 (250-m range hovering at 20-m elevation).

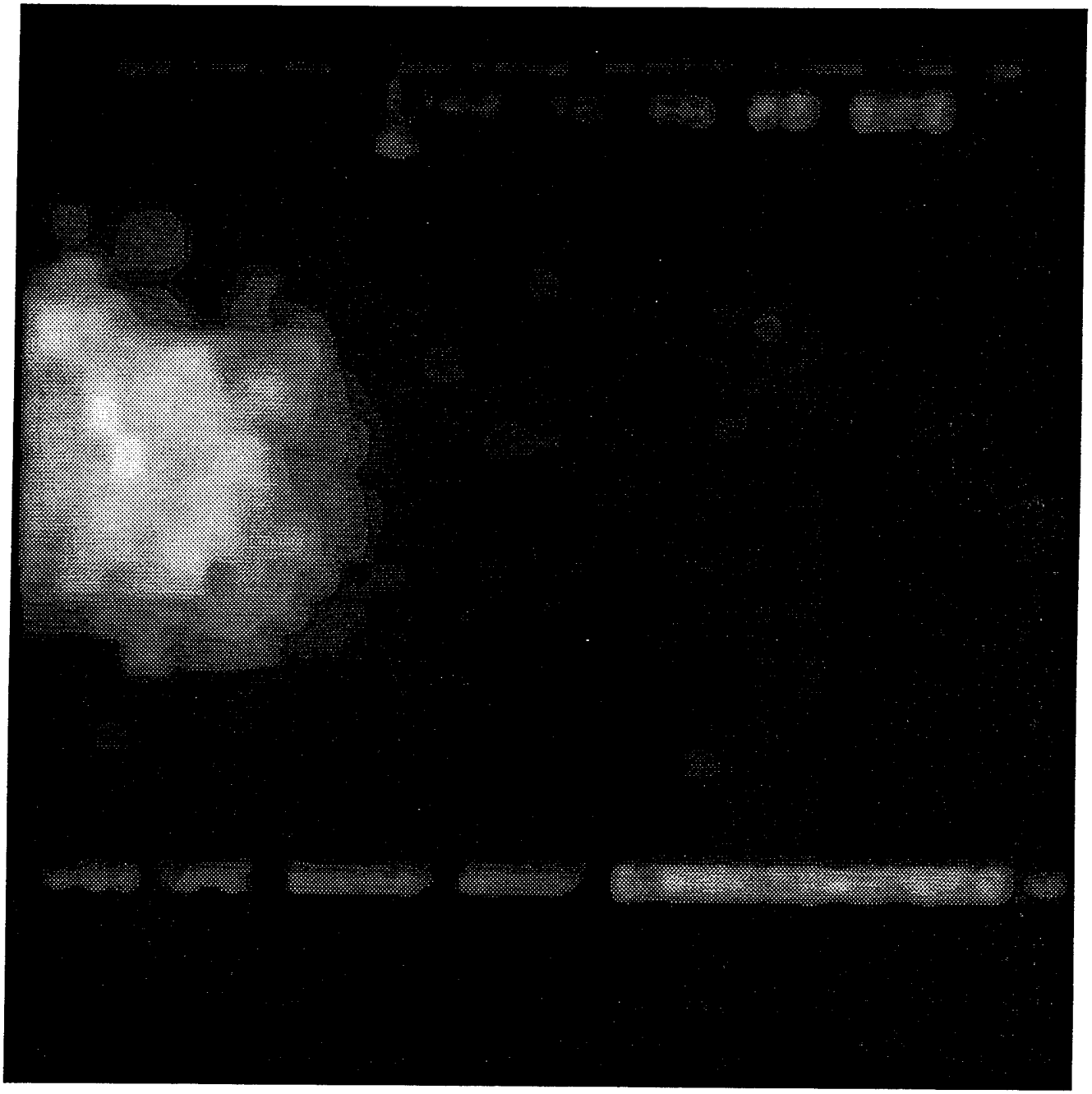

Figure 13. Thirty-frame smoothed and filtered image for trial 3 (250-m range hovering at 20-m elevation with the beam passing through the helicopter exhaust).

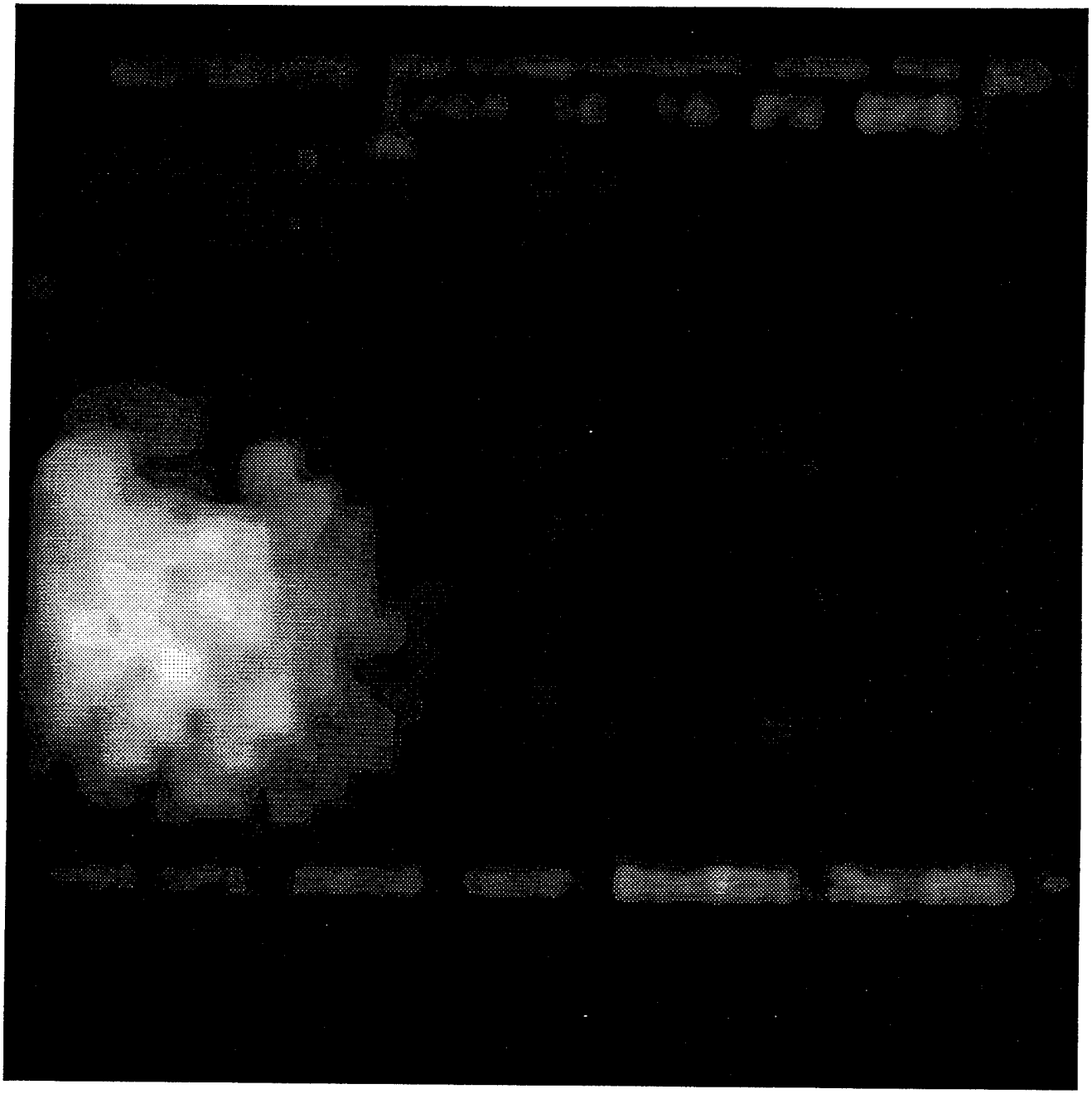

Figure 14. Thirty-frame smoothed and filtered image for trial 4 (250-m range hovering at 20-m elevation with the beam passing through the helicopter exhaust).

The effective diameter of the half-maximum beam for the two 20-m elevation hovering trials (4 and 5) from the June test yield an average value of 51.9 pixels. This test most closely compares to the August test's angular separations for the imager to target board and helicopter to target board. Extrapolation to the August test's 20-m hovering at 250-m range and with magnified image conditions yields an effective diameter of 63.2 pixels for trials 1 and 2. The corresponding half-maximum threshold areas for trials 1 and 2 are 11,770 and 10,577 pixels, respectively. The average effective diameter for the areas is 119.3 pixels. The enhanced sensitivity and beam characteristics have yielded a beam nearly twice the diameter. The corresponding vertical stretch factors are 1.28 and 1.38 for the June test trials and 1.31 and 1.28 for the August test trials, in excellent agreement for the close range, hovering helicopter case.

The results for trials 3 and 4 (hovering with the beam passing through the exhaust) were not consistent with the previous test. The June test trials 8 and 9 show an exhaust related area increase of a factor of 1.38 and a vertical stretch factor of 1.58; whereas, for August, the averaged corresponding values are 1.26 and 0.79. The discrepancy can be traced to the horizontal (with some vertical) beam displacement and a vertical compression with some horizontal stretch caused by the laser pointing mirrors. To collect data on the exhaust distorted beam, the imager line of sight had to be lowered slightly (50 pixels or ¼ m) to center the laser beam in the display image. The more significant horizontal displacement of nearly ½ m could not be completely taken into account. As a result, the left edge of the beam is clipped. More significant is the beam shape distortion introduced by the pointing mirrors. The beam is probably compressed in the vertical by a factor of 30 to 50 percent. Unfortunately, there was not enough time during the test to correct for the problem by moving the blackbody mirror to the upper center of the target board and redoing the appropriate trials, because of helicopter flight time and the refueling schedule.

4. Ground Level 500-m Range With and Without Turbulence (Trials 5, 6, and 7)

During the June test, a comparison of the helicopter on the ground with and without the rotor on was made between trial 1 and trials 2 and 3 (table 1). The beam area energy of the corresponding cases did not change appreciably for the 343-m range, although, there was an appreciable difference of the vertical stretch factors; a ratio of 1.40. The turbulence level was low; probably C_n^2 on the order of mid 10^{-14} $m^{-2/3}$ because of the strong 10-m/s winds.

During the August test, strong ground turbulence, C_n^2 of 10^{-13} $m^{-2/3}$, and moderate winds were present. The comparison of trials 5 and 6 with trial 7 illustrates the effect of the strong turbulence (see figures 15 to 17 with 80- to 90-frame averages). Also of significance is the nonGaussian beam intensity distribution that results in a smaller effective diameter for the half-maximum threshold intensity than in the 250-m trials (1 through 4); whereas, the overall beam extent can clearly be seen to have broadened by more than a factor of 2 (indicative of the 60 percent loss in beam energy shown in table 2). The trials also show little difference in the overall shape of the beam; but, the energy content has been reduced by 50 percent because of turbulence. This implies that the turbulence close to the laser has the most effect and the rotor jitter is of little consequence. This is slightly different than the June results that showed a 40 percent vertical stretch.

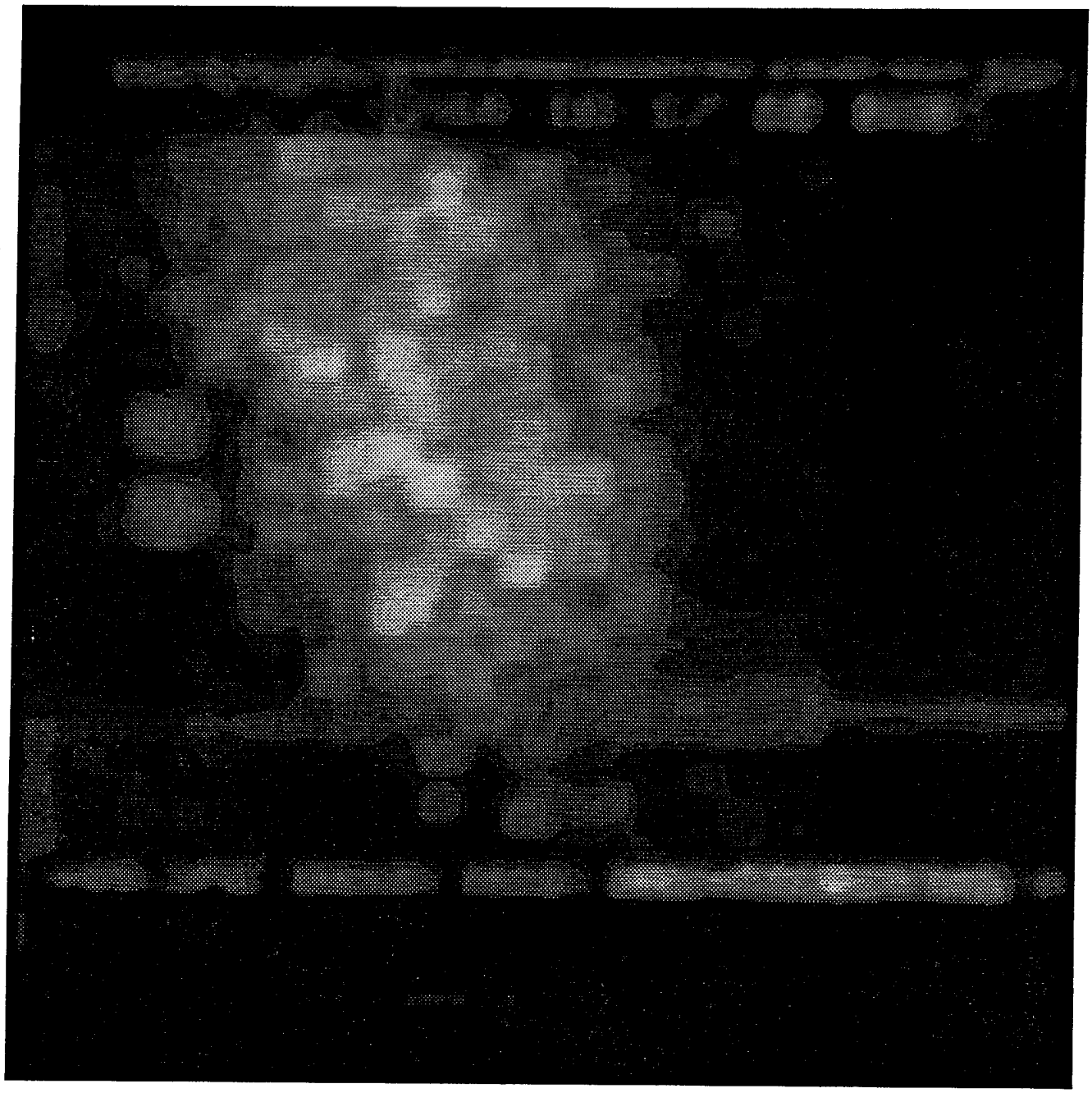

Figure 15. Eighty-frame smoothed and filtered image for trial 5 (500-m range on the ground with the rotors on).

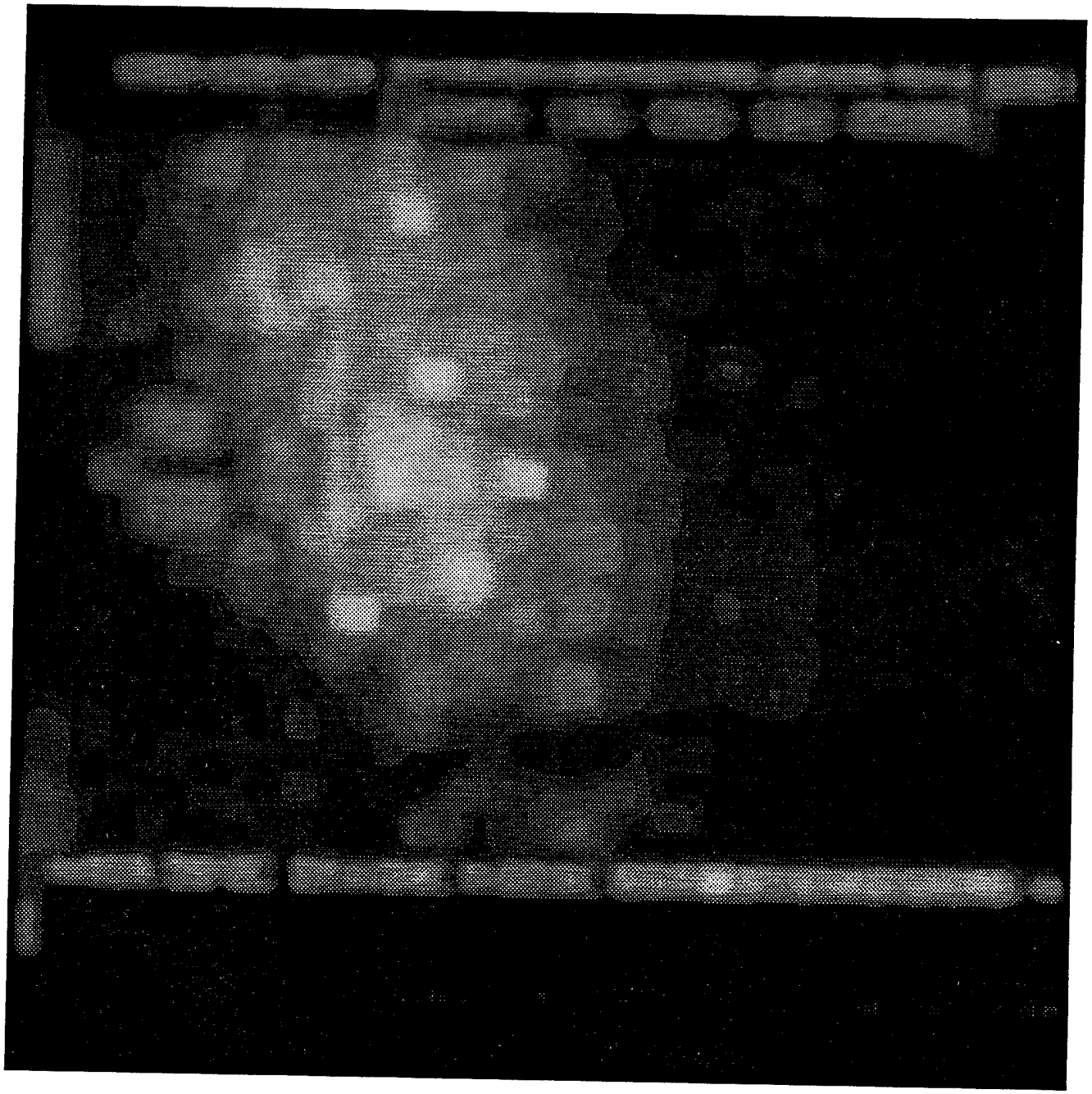

Figure 16. Eighty-frame smoothed and filtered image for trial 6 (500-m range on the ground with the rotors on).

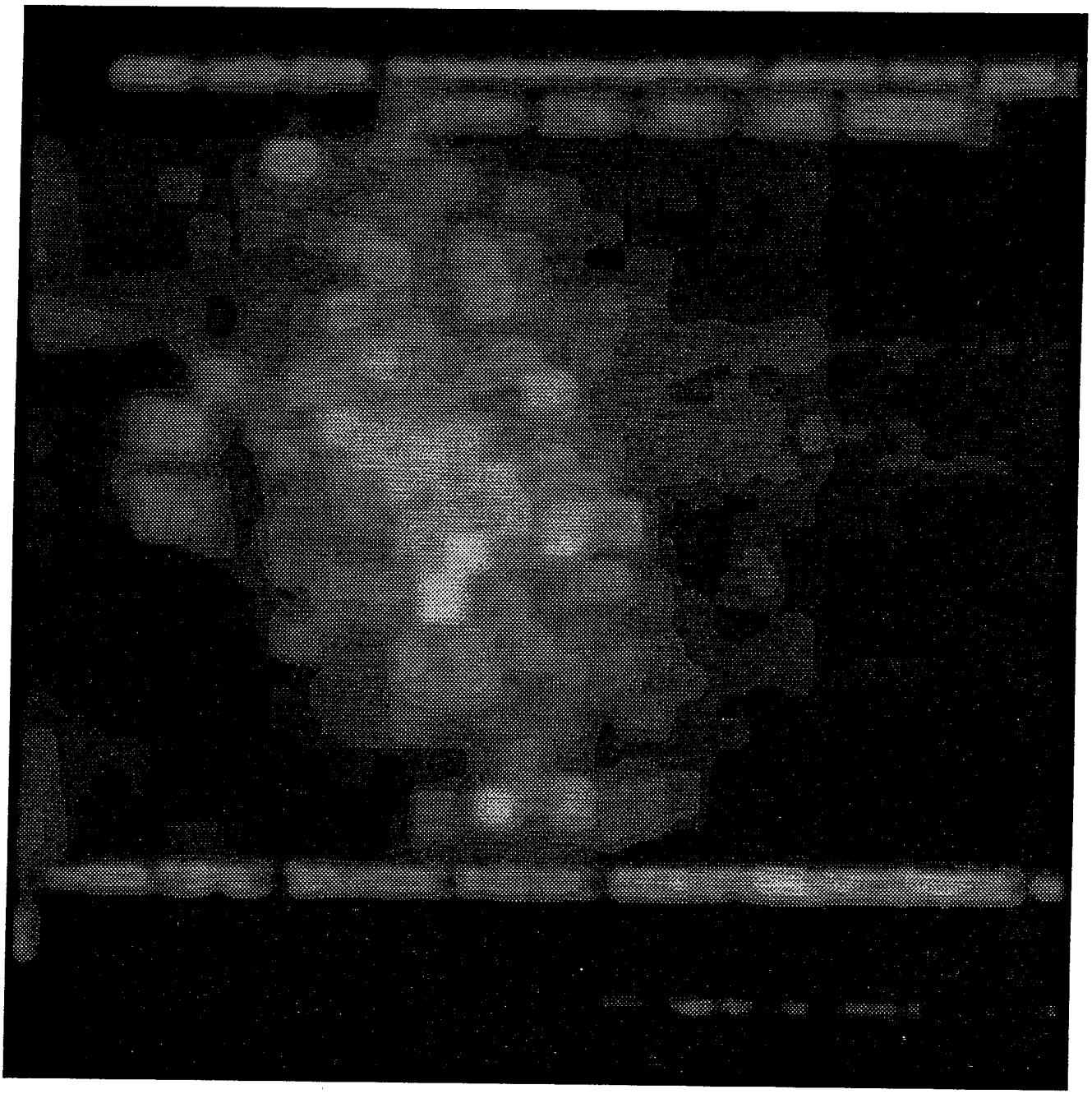

Figure 17. Ninety-frame smoothed and filtered image for trial 7 (500-m range on the ground with the rotors off).

5. Hovering 500-m Range (Trials 8 and 9)

During the June test, the effect of hovering versus the helicopter on the ground with the rotors on was a 10 percent increase in the vertical stretch of the beam and a 30 percent increase in the energy content from comparison of trials 2 and 3 with trials 4 and 5 for a 343-m range. The energy increase could be due to less overlap of the maximizing filtered and smoothed areas produced by the individual hot spots for the vertically elongated beam.

Results of the August test are somewhat different than the June test results. The comparison of trials 5 and 6 (figures 15 and 16) with trials 8 and 9 (figures 18 and 19 with 90-frame averages) show little difference in energy content and a slight horizontal broadening of the beam (a 5 percent reduction of the stretch factor). The beam at 500-m range was about a factor of two-thirds as large in both directions as the extrapolated beam profile for the June test (67-cm effective diameter at 500-m range in August versus 96-cm effective diameter at 500-m in June). The shrinking in diameter as a function of range is due to the loss of the relative beam energy content and disproportionate amount of area below the half-power GS level between the 250- and 500-m range helicopter positions. The influence of the laser-pointer optics is not known.

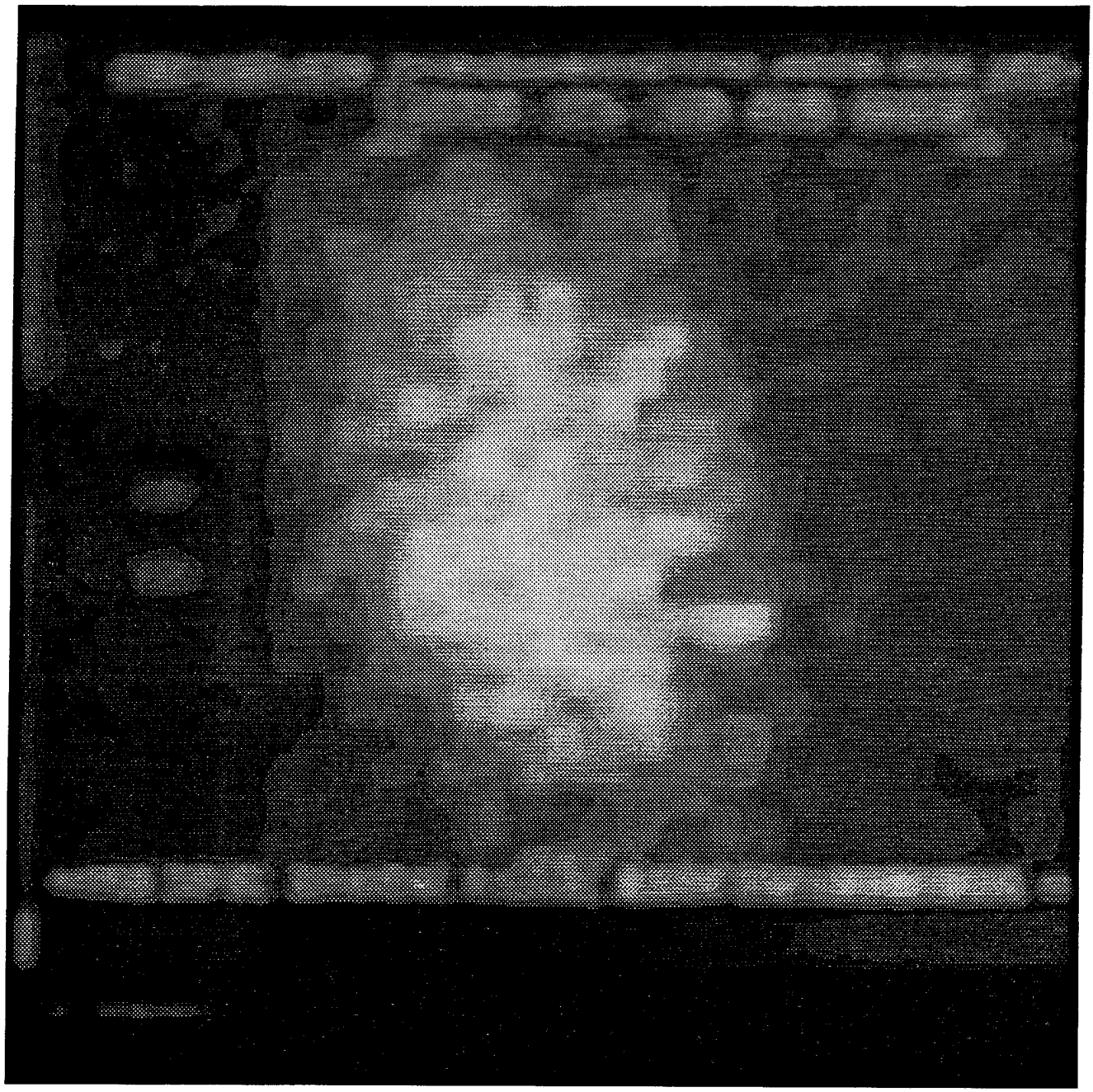

Figure 18. Ninety-frame smoothed and filtered image for trial 8 (500-m range hovering at 20-m elevation).

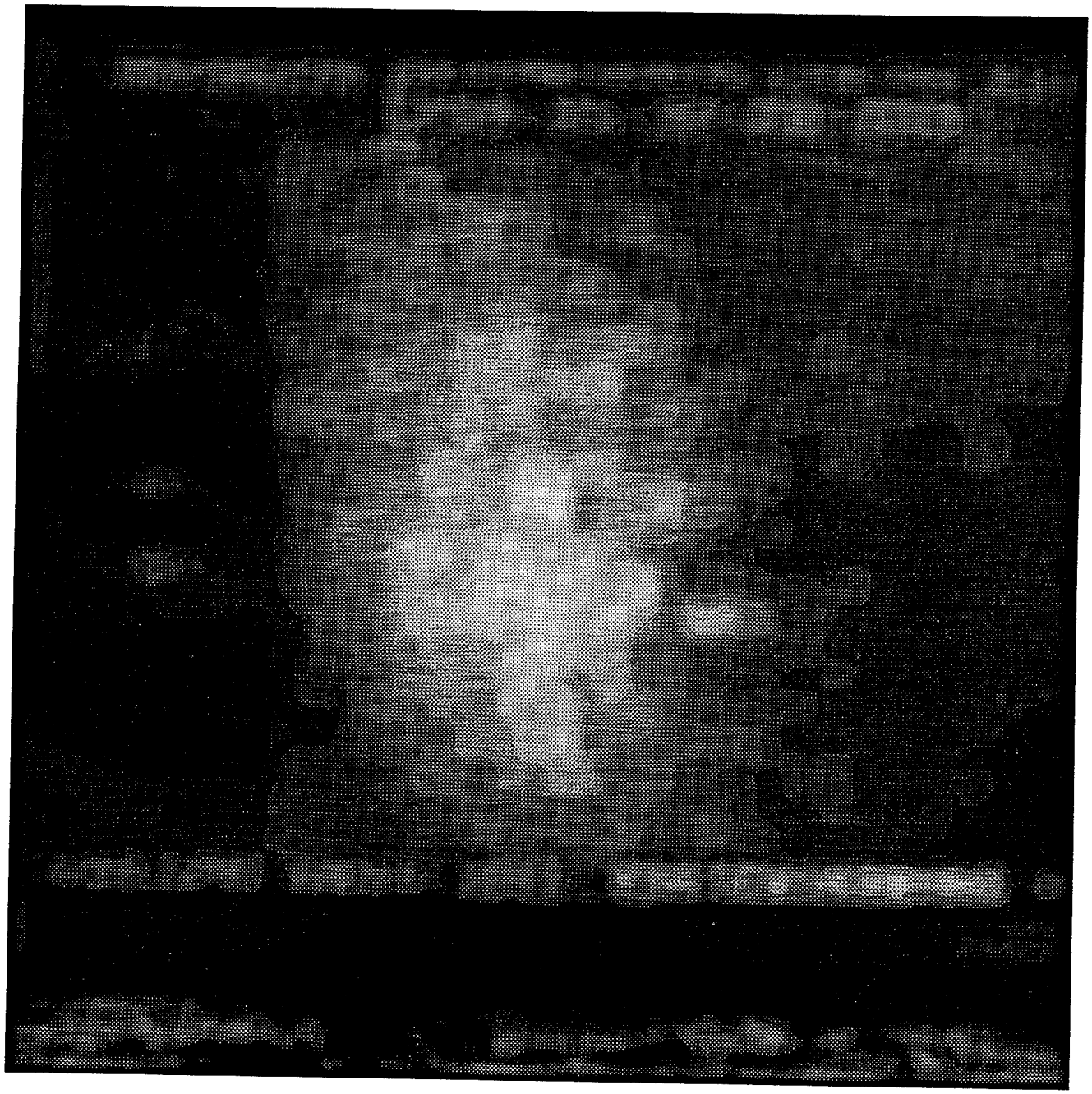

Figure 19. Ninety-frame smoothed and filtered image for trial 9 (500-m range hovering at 20-m elevation).

6. Hovering 500-m Range Through Exhaust (Trial 10)

The June test comparison of trials 8 and 9 at a 343-m range shows a vertical stretch and a substantial increase in beam energy (possibly associated with the analyses technique used for deriving beam geometry from isolated spots in consecutive laser beam images) caused by the laser beam passing through the helicopter exhaust.

The bimodal beam character associated with the laser beam that passed through the lower portion of the helicopter exhaust plume was not seen in June but was noted in the August test. The reason this was not previously noted could be the poorer sensitivity of the imager or positioning of the exhaust plume slightly to the side of the laser line of sight. The bimodal distribution can be seen by comparing trials 8 and 9 (figures 18 and 19) with trial 10 (figure 20 with a 90-frame average). The beam was translated about ½ m to the left and over ½ m down on the target board because of the laser pointing mirror. The beam is positioned horizontally in about the same place as in the 250-m range exhaust trials 3 and 4, because the angular horizontal pointing offset nearly cancels the horizontal skewing translation error caused by aiming the laser to the back instead of out the side of the helicopter. The two spots associated with the mirror holder are located in trial 10 in the upper left portion of the image with only the top spot isolated from the laser beam profile. As a result, the image of the beam passing through the exhaust plume is clipped on the left side and the bottom. The beam is stretched in the vertical and horizontal directions, but the amount cannot be accurately quantified because of the clipping.

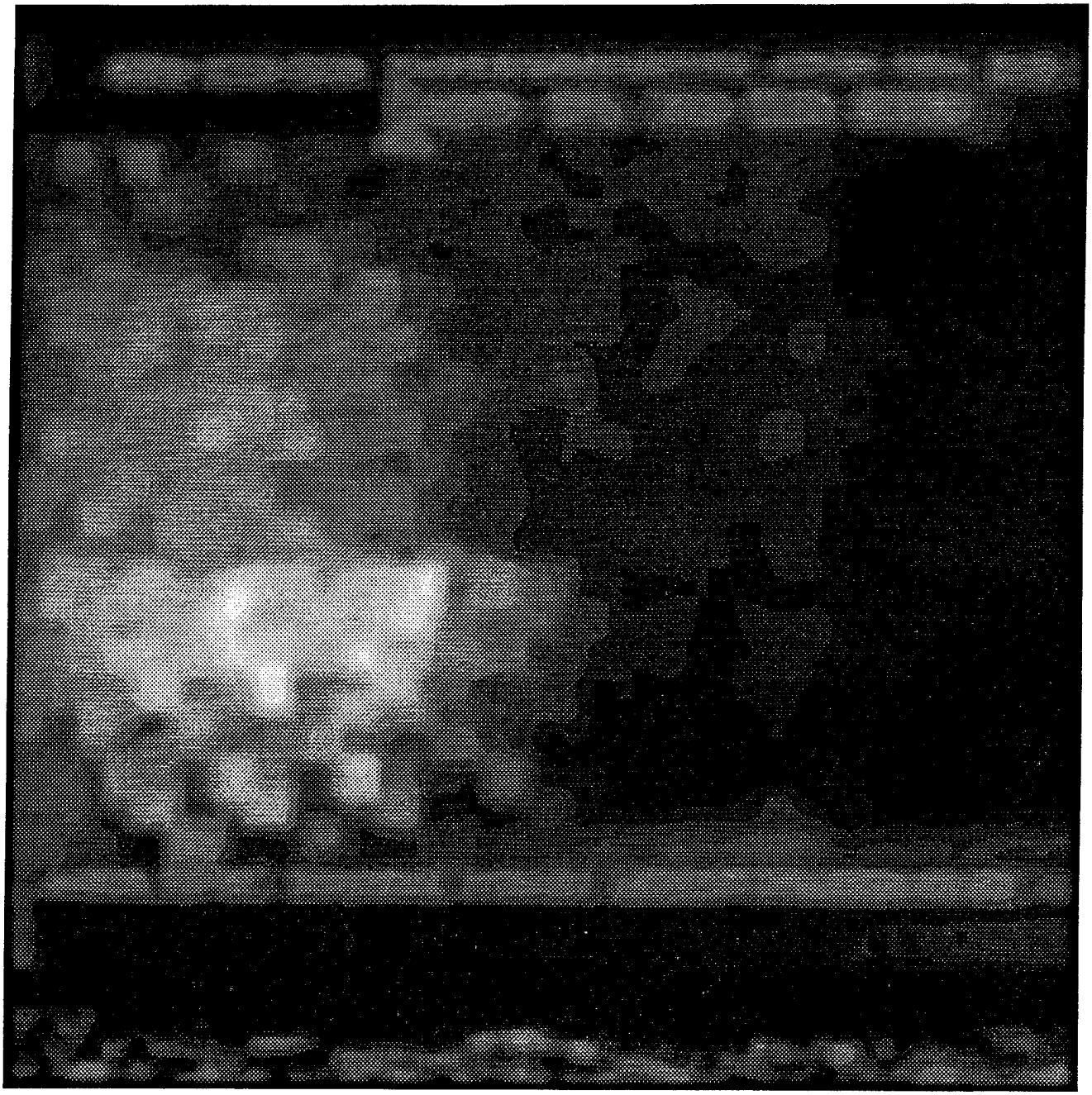

Figure 20. Ninety-frame smoothed and filtered image for trial 10 (500-m range hovering at 20-m elevation).

7. Hovering 750-m Range With and Without Exhaust (Trials 11 to 14)

The results of trials 11 to 14 do not have corresponding analogies from the June test. Trials 11 and 12 (figures 21 and 22 with 125-frame averages) are for 20-m elevation hovering at 750-m range. Trials 13 and 14 (figures 23 and 24 with 125-frame averages) are for 20-m elevation hovering at 750-m range through the helicopter exhaust. The images for trials 11 and 12 have beams that extend significantly above and below the target board vertical extent. The stronger, lower peak of the bimodal beam shape, probably, is due to ground reflections from the beam below the target board being deposited on the lower portion of the target. The bimodal mechanism is different than the one that produced the image for trial 10 in which the lower peak is not on the edge of the target board. For the exhaust plume trials, the skewing translation error caused the beam center to be below the target board; therefore, the presumed exhaust induced bimodal beam shape cannot be seen because the strong secondary peak in the beam would also be below the target board. The significant ground reflections of the beam below the target board produce a strong peak on the bottom of the target board image in figures 23 and 24. Additional tests are needed to characterize the extent and range dependence of the exhaust induced bimodal beam shape.

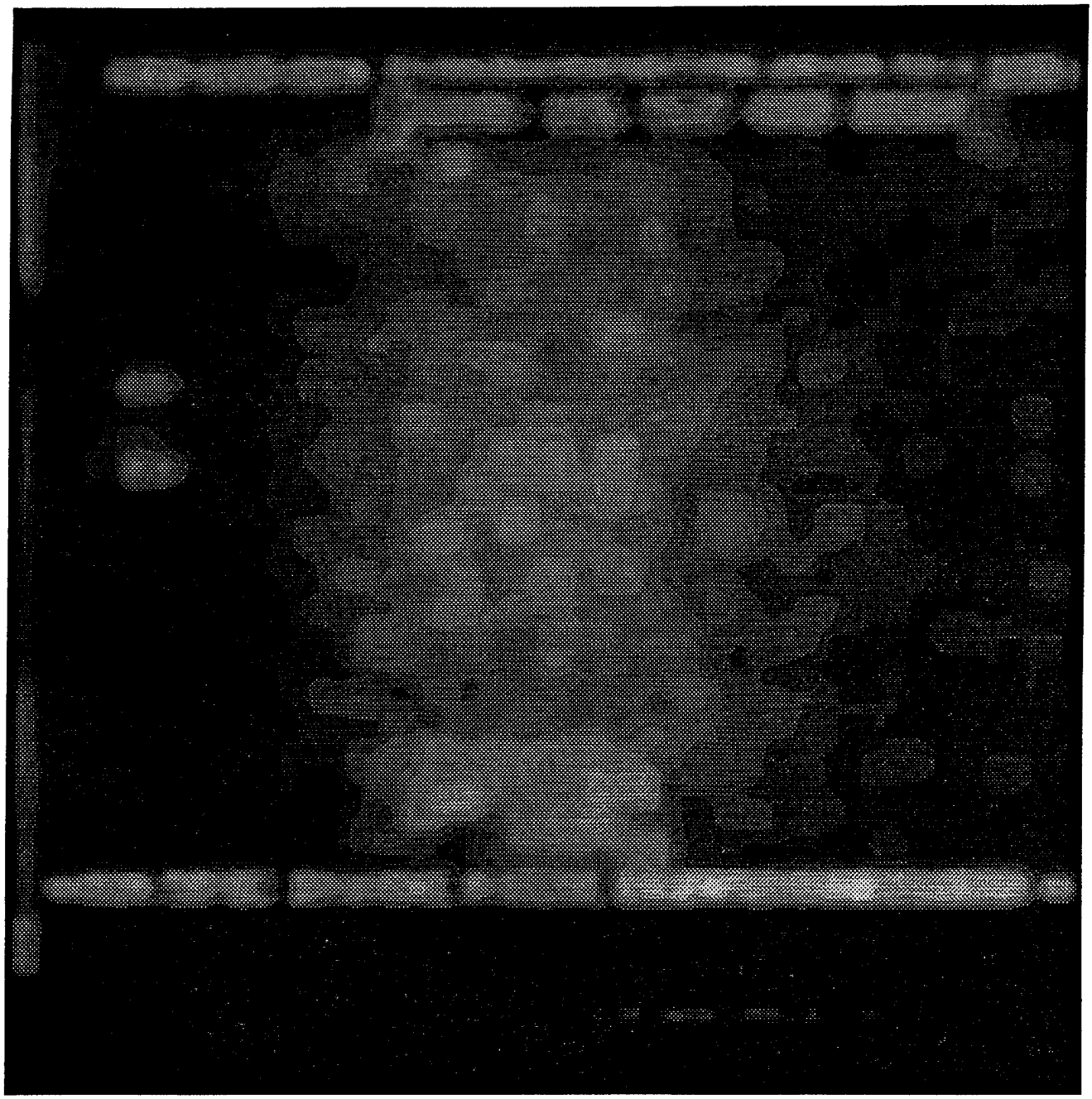

Figure 21. One hundred twenty five-frame smoothed and filtered image for trial 11 (750-m range hovering at 20-m elevation).

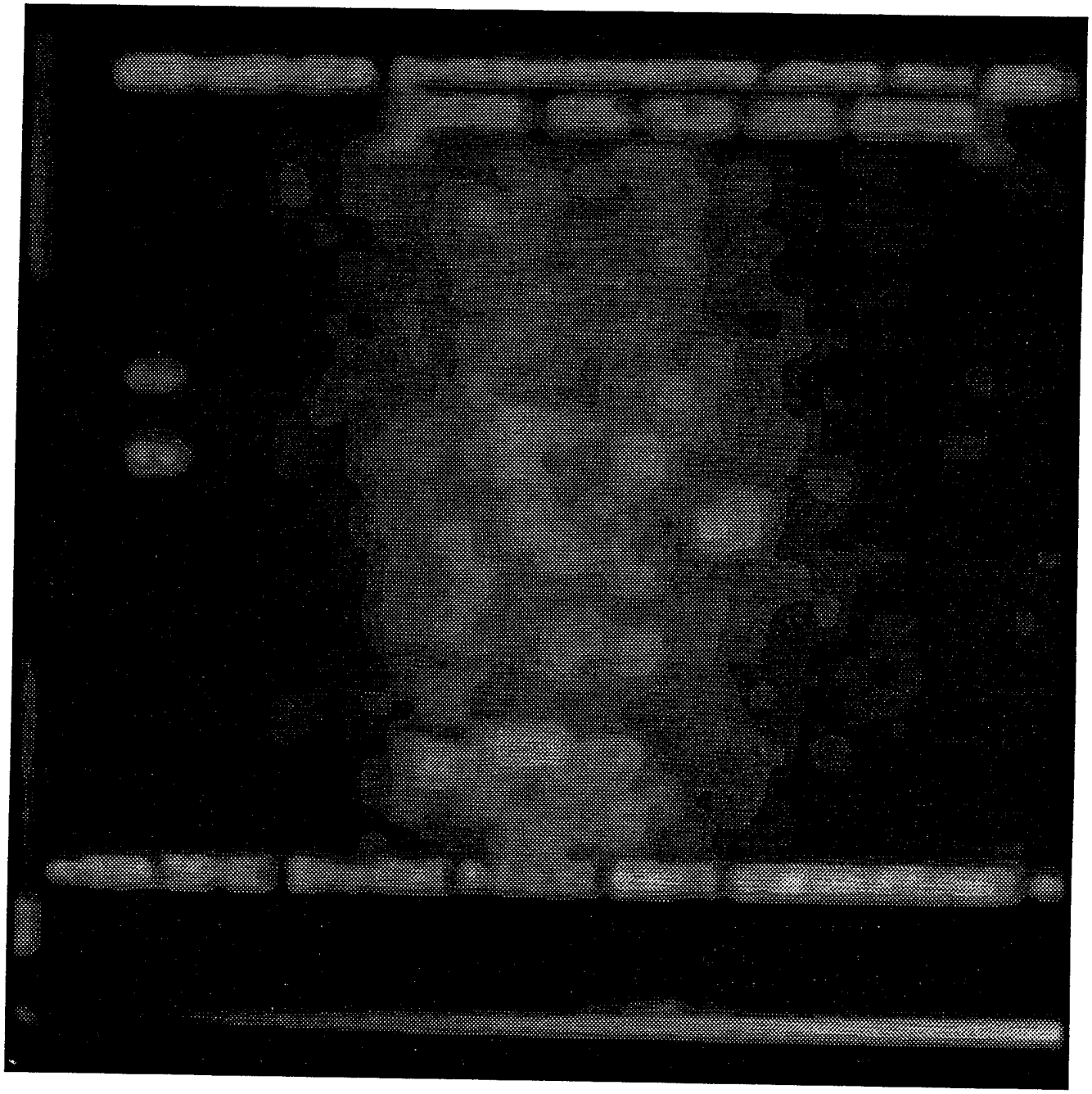

Figure 22. One hundred twenty five-frame smoothed and filtered image for trial 12 (750-m range hovering at 20-m elevation).

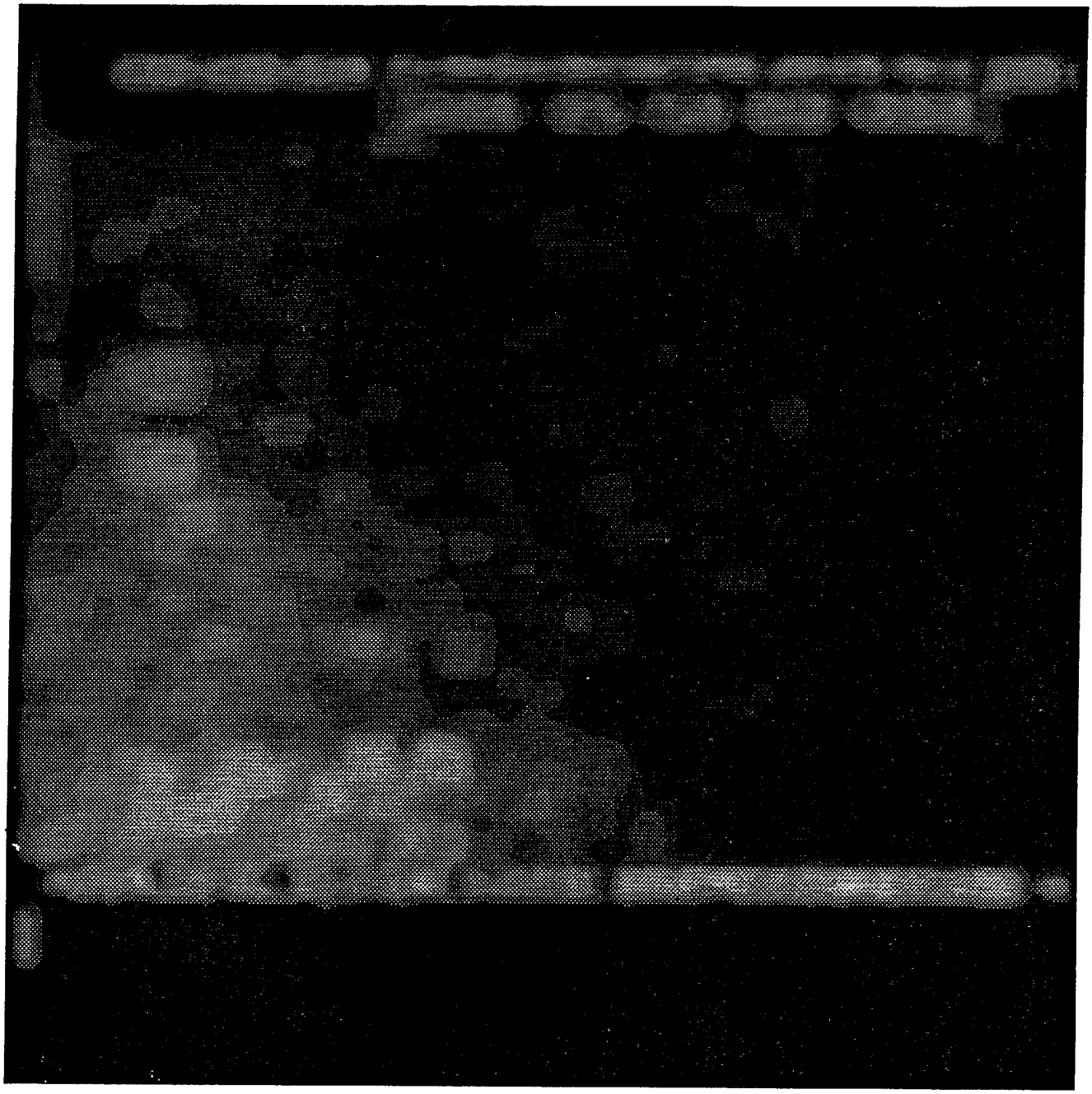

Figure 23. Fifty-frame smoothed and filtered image for trial 13 (750-m range hovering at 20-m elevation with the beam passing through the helicopter exhaust).

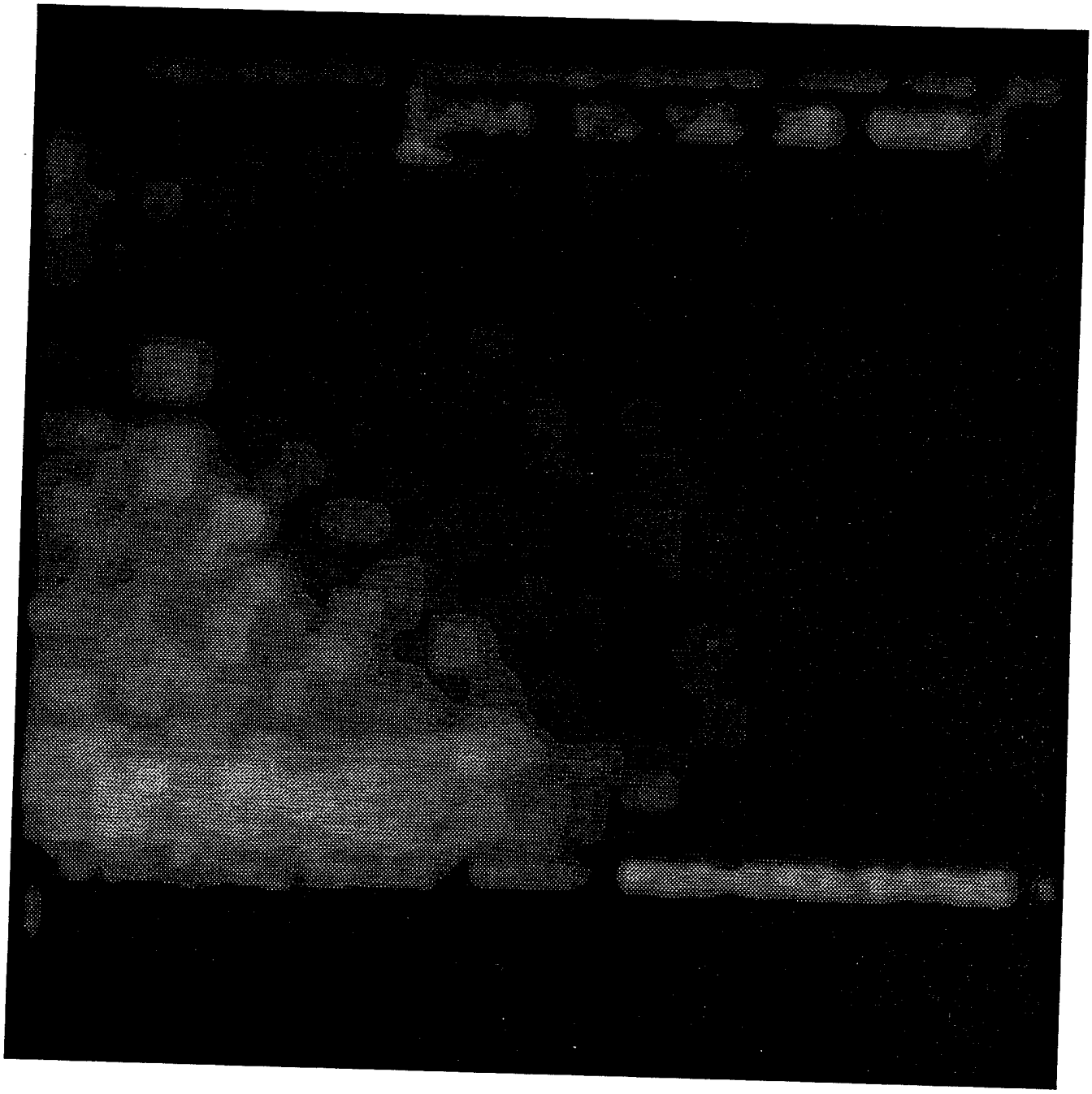

Figure 24. One hundred-frame smoothed and filtered image for trial 14 (750-m range hovering at 20-m elevation with the beam passing through the helicopter exhaust).

8. Conclusions

Table 2 summarizes the results from the August test. Table 1 shows the results from the June test. The laser beam for the August test had four times the area of the June test. Some of this increase could be the result of the improved sensitivity and resolution used in the August test via the 6.7X telescope used. The August test beam had a 60 percent vertical stretch (trial 7) reduced slightly by the rotors being turned as well as hovering in the air. Passing through the exhaust caused varying results, depending on the range. At the short range (250 m), the beam was compressed in the vertical. At the intermediate range (500 m), the beam became bimodal. At the long range (750 m), the beam fell predominately below the scattering target board, so no profile information was obtained. Note the 50 percent energy loss between the ground level 500-m-range trials with and without the rotors on, presumably, from the strong optical turbulence that predominately affects the beam close to the helicopter. Also, passing the beam through the helicopter exhaust caused the beam to distort but gave localized enhancement of the beam energy content. This phenomenon needs additional data for assessment because the laser beam and target board were not optimal for characterization of its range dependence.

References

Crow, S. B., W. R. Watkins, F. R. Palacios, and D. R. Billingsley, "Technique for Measuring Atmospheric Effects on Image Metrics." In *Proceedings SPIE*, 1486:333, 1991.

Jordan, J. B., private conversation, Department of Electrical and Computer Engineering, New Mexico State University, Las Cruces, NM, July 1994.

Kantrowitz, F. T., W. R. Watkins, D. R. Billingsley, and F. R. Palacios, "Characterization, Propagation, and Simulation of the Infrared Scenes." In *Proceedings SPIE*, 1311:180, 1990.

Model 610 Operations Manual, Inframetrics, Inc., 1983.

Palacios, F. R., W. R. Watkins, S. B. Crow, and D. R. Billingsley, "Correlation of C_n^2 with Image Distortion at the REBAL Test." In *Proceedings Battlefield Atmospherics Conference*, 1992.

Palacios, F. R., W. R. Watkins, S. B. Crow, D. R. Billingsley, *Helicopter-Mounted Laser Beam Characterization Test*, Army Research Laboratory, White Sands Missile Range, NM, 1994.

Watkins, W. R., F. T. Kantrowitz, and S. B. Crow, "Transmission Measurements With the Target Contrast Characterizer." In *Proceedings SPIE*, 1115:179, 1989.

Acronyms and Abbreviations

FWHM	full width at half maximum
GS	grayscale
HAFB	Holloman Air Force Base
IR	infrared

Distribution

	Copies
NASA MARSHAL SPACE FLT CTR ATMOSPHERIC SCIENCES DIV E501 ATTN DR FICHTL HUNTSVILLE AL 35802	1
NASA SPACE FLT CTR ATMOSPHERIC SCIENCES DIV CODE ED 41 1 HUNTSVILLE AL 35812	1
ARMY STRAT DEFNS CMND CSSD SL L ATTN DR LILLY PO BOX 1500 HUNTSVILLE AL 35807-3801	1
ARMY MISSILE CMND AMSMI RD AC AD ATTN DR PETERSON REDSTONE ARSENAL AL 35898-5242	1
ARMY MISSILE CMND AMSMI RD AS SS ATTN MR H F ANDERSON REDSTONE ARSENAL AL 35898-5253	1
ARMY MISSILE CMND AMSMI RD AS SS ATTN MR B WILLIAMS REDSTONE ARSENAL AL 35898-5253	1
ARMY MISSILE CMND AMSMI RD DE SE ATTN MR GORDON LILL JR REDSTONE ARSENAL AL 35898-5245	1
ARMY MISSILE CMND REDSTONE SCI INFO CTR AMSMI RD CS R DOC REDSTONE ARSENAL AL 35898-5241	1

ARMY MISSILE CMND 1
AMSMI
REDSTONE ARSENAL
AL 35898-5253

ARMY INTEL CTR 1
AND FT HUACHUCA
ATSI CDC C
FT HUACHUCA AZ 85613-7000

CMD 420000D C0245 1
ATTN DR A SHLANTA
NAVAIRWARCENWPNDIV
1 ADMIN CIR
CHINA LAKE CA 93555-6001

PACIFIC MISSILE TEST CTR 1
GEOPHYSICS DIV
ATTN CODE 3250
POINT MUGU CA 93042-5000

LOCKHEED MIS & SPACE CO 1
ATTN KENNETH R HARDY
ORG 91 01 B 255
3251 HANOVER STREET
PALO ALTO CA 94304-1191

NAVAL OCEAN SYST CTR 1
CODE 54
ATTN DR RICHTER
SAN DIEGO CA 92152-5000

METEOROLOGIST IN CHARGE 1
KWAJALEIN MISSILE RANGE
PO BOX 67
APO SAN FRANCISCO
CA 96555

DEPT OF COMMERCE CTR 1
MOUNTAIN ADMINISTRATION
SPPRT CTR LIBRARY R 51
325 S BROADWAY
BOULDER CO 80303

DR HANS J LIEBE 1
NTIA ITS S 3
325 S BROADWAY
BOULDER CO 80303

NCAR LIBRARY SERIALS
NATL CTR FOR ATMOS RSCH
PO BOX 3000
BOULDER CO 80307-3000 1

DEPT OF COMMERCE CTR
325 S BROADWAY
BOULDER CO 80303 1

DAMI POI
WASH DC 20310-1067 1

MIL ASST FOR ENV SCI OFC
OF THE UNDERSEC OF DEFNS
FOR RSCH & ENGR R&AT E LS
PENTAGON ROOM 3D129
WASH DC 20301-3080 1

DEAN RMD
ATTN DR GOMEZ
WASH DC 20314 1

ARMY INFANTRY
ATSH CD CS OR
ATTN DR E DUTOIT
FT BENNING GA 30905-5090 1

AIR WEATHER SERVICE
TECH LIBRARY FL4414 3
SCOTT AFB IL 62225-5458 1

USAFETAC DNE
ATTN MR GLAUBER
SCOTT AFB IL 62225-5008 1

HQ AWS DOO 1
SCOTT AFB IL 62225-5008 1

PHILLIPS LABORATORY
PL LYP
ATTN MR CHISHOLM
HANSCOM AFB MA 01731-5000 1

ATMOSPHERIC SCI DIV
GEOPHYSICS DIRCTRT
PHILLIPS LABORATORY
HANSCOM AFB MA 01731-5000 1

PHILLIPS LABORATORY
PL LYP 3
HANSCOM AFB MA 01731-5000 1

RAYTHEON COMPANY 1
ATTN DR SONNENSCHEIN
528 BOSTON POST ROAD
SUDBURY MA 01776
MAIL STOP 1K9

ARMY MATERIEL SYST 1
ANALYSIS ACTIVITY
AMXSY
ATTN MP H COHEN
APG MD 21005-5071

ARMY MATERIEL SYST 1
ANALYSIS ACTIVITY
AMXSY AT
ATTN MR CAMPBELL
APG MD 21005-5071

ARMY MATERIEL SYST 1
ANALYSIS ACTIVITY
AMXSY CR
ATTN MR MARCHET
APG MD 21005-5071

ARL CHEMICAL BIOLOGY 1
NUC EFFECTS DIV
AMSRL SL CO
APG MD 21010-5423

ARMY MATERIEL SYST 1
ANALYSIS ACTIVITY
AMXSY
APG MD 21005-5071

ARMY MATERIEL SYST 1
ANALYSIS ACTIVITY
AMXSY CS
ATTN MR BRADLEY
APG MD 21005-5071

ARMY RESEARCH LABORATORY 1
AMSRL D
2800 POWDER MILL ROAD
ADELPHI MD 20783-1145

ARMY RESEARCH LABORATORY 1
AMSRL OP SD TP
TECHNICAL PUBLISHING
2800 POWDER MILL ROAD
ADELPHI MD 20783-1145

ARMY RESEARCH LABORATORY
AMSRL OP CI SD TL
2800 POWDER MILL ROAD
ADELPHI MD 20783-1145 1

ARMY RESEARCH LABORATORY
AMSRL SS SH
ATTN DR SZTANKAY
2800 POWDER MILL ROAD
ADELPHI MD 20783-1145 1

ARMY RESEARCH LABORATORY
AMSRL
2800 POWDER MILL ROAD
ADELPHI MD 20783-1145 1

NATIONAL SECURITY AGCY W21
ATTN DR LONGBOTHUM
9800 SAVAGE ROAD
FT GEORGE G MEADE
MD 20755-6000 1

OIC NAVSWC
TECH LIBRARY CODE E 232
SILVER SPRINGS
MD 20903-5000 1

ARMY RSRC OFC
AMXRO GS
ATTN DR BACH
PO BOX 12211
RTP NC 27709 1

DR JERRY DAVIS
NCSU
PO BOX 8208
RALEIGH NC 27650-8208 1

US ARMY CECRL
CECRL GP
ATTN DR DETSCH
HANOVER NH 03755-1290 1

ARMY ARDEC
SMCAR IMI I BLDG 59
DOVER NJ 07806-5000 1

ARMY SATELLITE COMM AGCY
DRCPM SC 3
FT MONMOUTH NJ 07703-5303 1

ARMY COMMUNICATIONS
ELECTR CTR FOR EW RSTA
AMSEL EW D
FT MONMOUTH NJ 07703-5303 1

ARMY COMMUNICATIONS
ELECTR CTR FOR EW RSTA
AMSEL EW MD
FT MONMOUTH NJ 07703-5303 1

ARMY DUGWAY PROVING GRD
STEDP MT DA L 3
DUGWAY UT 84022-5000 1

ARMY DUGWAY PROVING GRD
STEDP MT M
ATTN MR BOWERS
DUGWAY UT 84022-5000 1

DEPT OF THE AIR FORCE
OL A 2D WEATHER SQUAD MAC
HOLLOMAN AFB
NM 88330-5000 1

PL WE
KIRTLAND AFB NM
87118-6008 1

USAF ROME LAB TECH
CORRIDOR W STE 262 RL SUL
26 ELECTR PKWY BLD 106
GRIFFISS AFB
NY 13441-4514 1

AFMC DOW
WRIGHT PATTERSON AFB
OH 0334-5000 1

ARMY FIELD ARTLLRY SCHOOL
ATSF TSM TA
FT SILL OK 73503-5600 1

NAVAL AIR DEV CTR
CODE 5012
ATTN AL SALIK
WARMINISTER PA 18974 1

ARMY FOREGN SCI TECH CTR
CM
220 7TH STREET NE
CHARLOTTESVILLE
VA 22901-5396 1

NAVAL SURFACE WEAPONS CTR
CODE G63
DAHLGREN VA 22448-5000 1

ARMY OEC
CSTE EFS
PARK CENTER IV
4501 FORD AVE
ALEXANDRIA VA 22302-1458 1

ARMY CORPS OF ENGRS
ENGR TOPOGRAPHICS LAB
ETL GS LB
FT BELVOIR VA 22060 1

TAC DOWP
LANGLEY AFB
VA 23665-5524 1

ARMY TOPO ENGR CTR
CETEC ZC 1
FT BELVOIR VA 22060-5546 1

LOGISTICS CTR
ATCL CE
FT LEE VA 23801-6000 1

SCI AND TECHNOLOGY
101 RESEARCH DRIVE
HAMPTON VA 23666-1340 1

ARMY NUCLEAR CML AGCY
MONA ZB BLDG 2073
SPRINGFIELD VA 22150-3198 1

USATRADOC
ATCD FA
FT MONROE VA 23651-5170 1

ARMY TRADOC ANALYSIS CTR
ATRC WSS R
WSMR NM 88002-5502 1

ARMY RESEARCH LABORATORY
AMSRL BE S
BATTLEFIELD ENVIR DIR
WSMR NM 88002-5501 1

ARMY RESEARCH LABORATORY
AMSRL BE W
BATTLEFIELD ENVIR DIR
WSMR NM 88002-5501 1

ARMY RESEARCH LABORATORY AMSRL BE ATTN MR VEAZY BATTLEFIELD ENVIR DIR WSMR NM 88002-5501	1
DTIC 8725 JOHN J KINGMAN RD SUITE 0944 FT BELVOIR VA 22060-6218	1
ARMY MISSILE CMND AMSMI REDSTONE ARSENAL AL 35898-5243	1
ARMY DUGWAY PROVING GRD STEDP 3 DUGWAY UT 84022-5000	1
USATRADOC ATCD FA FT MONROE VA 23651-5170	1
WSMR TECH LIBRARY BR STEWS IM IT WSMR NM 88001	1
Record Copy	2
TOTAL	79